Human coronaviruses disassemble processing bodies

Mariel Kleer[1,2,3*], Rory P. Mulloy[1,2,3*], Carolyn-Ann Robinson[1,2,3], Maxwell Bui-Marinos[1,2,3], Elizabeth L. Castle[4], Arinjay Banerjee[5,6,7], Samira Mubareka[8,9], Karen Mossman[10,11] and Jennifer A. Corcoran[1,2,3 #]

[1]Microbiology, Immunology and Infectious Diseases Department, University of Calgary, Calgary, AB, Canada.
[2]Charbonneau Cancer Research Institute, University of Calgary, Calgary, AB, Canada.
[3]Snyder Institute for Chronic Diseases, University of Calgary, Calgary, AB, Canada.
[4]School of Biomedical Engineering, University of British Columbia, Vancouver, BC, Canada.
[5]Vaccine and Infectious Disease Organization, University of Saskatchewan; Saskatoon, SK, Canada
[6]Department of Veterinary Microbiology, Western College of Veterinary Medicine, University of Saskatchewan; Saskatoon, SK, Canada
[7]Department of Biology, University of Waterloo; Waterloo, ON, Canada
[8]Department of Laboratory Medicine and Pathobiology, University of Toronto, Toronto, ON, Canada
[9]Sunnybrook Research Institute, Toronto, ON, Canada
[10]Department of Medicine, Master University, Hamilton, ON, Canada
[11]Institute for Infectious Disease Research, McMaster University, Hamilton, ON, Canada

[*]Equal contribution
[#]Corresponding Author

38 **Abstract**

39 The *Coronaviridae* are a family of viruses with large RNA genomes. Seven coronaviruses
40 (CoVs) have been shown to infect humans, including the recently emerged severe acute
41 respiratory syndrome coronavirus 2 (SARS-CoV-2), the causative agent of coronavirus disease
42 (COVID-19). The host response to CoV infection is complex and regulated, in part, by
43 intracellular antiviral signaling pathways triggered in infected cells. Pathogenic CoVs can hijack
44 these antiviral responses, reshaping the production of interferons and proinflammatory cytokines.
45 Processing bodies (PBs) are membraneless ribonucleoprotein granules that mediate decay or
46 translational suppression of cellular mRNAs; this is particularly relevant for proinflammatory
47 cytokine mRNA which normally reside in PBs and are repressed. PBs or their components are
48 believed to play important direct-acting antiviral roles, providing a compelling reason for their
49 frequent disassembly by many viruses. Prior to this report, no information was known about how
50 human CoVs impact PBs. Here, we show that three human CoVs, SARS-CoV-2 and the
51 common cold CoVs, OC43 and 229E, induce PB loss. Moreover, we screened a SARS-CoV-2
52 gene library and identified that expression of the viral nucleocapsid (N) protein from SARS-
53 CoV-2 was sufficient to mediate PB disassembly. N protein mediated PB loss correlated with
54 elevated transcript levels of selected proinflammatory cytokines that would normally be
55 repressed in PBs. Ectopic expression of the N proteins from four other human coronaviruses
56 (OC43, MERS, 229E and NL63) did not cause PB disassembly, suggesting that this feature is
57 unique to SARS-CoV-2 N protein. These data indicate that SARS-CoV-2 disassembles PBs
58 during infection. As an unintended side effect, the disassembly of PBs may enhance levels of
59 proinflammatory cytokine mRNAs which normally reside in PBs, thereby reshaping the
60 subsequent immune response.

61 **Introduction**

62 Processing bodies (PBs) are membraneless ribonucleoprotein (RNP) granules found in the
63 cytoplasm of all cells [1,2]. PBs control cellular gene expression because they either degrade or
64 sequester cellular RNA transcripts, preventing their translation into protein. PBs contain many
65 enzymes required for mRNA turnover, including those needed for decapping (Dcp2 and co-
66 factors Dcp1a and Edc4/Hedls) and decay of the RNA body (5'-3' exonuclease Xrn1 and RNA
67 helicase Rck/DDX6) and some components of the RNA-induced silencing complex [3,4]. Not all
68 coding RNAs are regulated by PBs, but those that are typically encode potent regulatory
69 molecules like growth factors, pro-inflammatory cytokines, and angiogenic factors. One group of
70 protein-coding mRNAs commonly found in PBs bear destabilizing AU-rich elements (AREs) in
71 their 3'-untranslated regions (3'-UTRs) and include most proinflammatory cytokine transcripts
72 [5-7]. These RNAs shuttle to PBs by virtue of interactions between the AU-rich element and
73 RNA-binding proteins (RBPs). Once localized to PBs, most RNA transcripts are unable to
74 undergo translation, although in rare cases translation repression can be reversible [3,8-11]. We
75 and others showed that the presence of PBs correlates with increased turnover/suppression of
76 ARE-mRNAs [7,12-15]. Conversely, when PBs are lost, constitutive ARE-mRNA suppression is
77 reversed, and ARE-mRNA transcripts and/or their translation products accumulate. Therefore,
78 PB disassembly can be viewed as a switch that permits cells to rapidly respond and translate
79 ARE-containing proinflammatory cytokine RNA into molecules such as IL-6, IL-8, IL-1β, and
80 TNF [5]. PBs provide an extra layer of post-transcriptional control enabling the cell to fine tune
81 the production of potent molecules like proinflammatory cytokines.

82

83 Although PBs are constitutive, they are also dynamic, changing in size and number in response
84 to different stimuli or stressors. This dynamic disassembly/assembly is possible because PBs

85 behave as biomolecular condensates that form via liquid-liquid phase separation of proteins [16-
86 19]. PBs form via sequential multivalent RNA-protein interactions, with a small group of
87 proteins that contain regions of intrinsic disorder serving as the essential scaffold onto which
88 additional proteins or RNA can be recruited as the PB matures [9,16,20-24]. Despite the
89 recognition of PBs as dynamic entities, our understanding of the signals that induce PB
90 disassembly remains incomplete. We and others have shown that stressors which activate the
91 p38/MK2 MAP kinase pathway, as well as many virus infections elicit PB disassembly
92 [12,13,15,25,26]. Disassembly can occur by a direct interaction between a viral protein(s) and a
93 PB component that is subsequently re-localized to viral replication and transcription
94 compartments (vRTCs) [27-29] or cleaved by viral proteases [30-32]. Viruses can also cause PB
95 disassembly indirectly by activating p38/MK2 signaling [12,13,26].
96
97 There are numerous reports of viral gene products that trigger PB disassembly, yet corresponding
98 reports of viral gene products that stimulate PB formation are rare, suggesting that PBs possess
99 direct antiviral function and their disassembly may favour viral replication in ways that we do
100 not yet grasp [33,34]. Even though other RNPs, such as stress granules, have emerged as
101 important components of our antiviral defenses that contribute to sensing virus and triggering
102 innate immune responses, evidence to support a direct antiviral role for PBs is less well
103 established [34-37]. A direct-acting antiviral role has been defined for several PB-localized
104 enzymes that impede viral replication (e.g. APOBEC3G, MOV10). However, in these cases, the
105 mechanism of viral restriction was attributed to the enzymatic activity of the PB protein(s)
106 whereas its localization to PBs was not deemed as significant [28,29,31,38-45]. Nonetheless, the
107 disassembly of PBs by diverse viruses strongly suggests they negatively regulate virus

108 replication, though it does create the following paradox. The reason viruses disassemble PBs
109 may be to limit their antiviral activity; however, because PBs also control turnover/suppression
110 of many proinflammatory cytokine transcripts, their disruption by viruses contributes to high
111 proinflammatory cytokine levels as an unintended consequence.
112
113 The family *Coronaviridae* includes seven viruses that infect humans, including the four
114 circulating 'common cold' coronaviruses (CoVs), HCoV-OC43, HCoV-229E, HCoV-NL63, and
115 HCoV-HKU1 and three highly pathogenic viruses that cause severe disease in humans: MERS-
116 CoV, SARS-CoV, and the recently emerged SARS-CoV-2 [46-51]. Severe COVID-19 is
117 characterized by aberrant proinflammatory cytokine production, endothelial cell (EC)
118 dysfunction and multiple organ involvement [52-64]. Even with intense study, we do not yet
119 appreciate precisely how SARS-CoV-2 infection causes severe COVID-19 in some patients and
120 mild disease in others though a mismanaged or delayed IFN response and an overactive cytokine
121 response is thought to underlie severe outcomes [65-70]. Despite some contrasting reports, [71-
122 73], what is clear is that SARS-CoV-2 proteins use a multitude of mechanisms to outcompete
123 cellular antiviral responses [68,74-85].
124
125 To determine if SARS-CoV-2 and other CoVs interact with PBs to alter the cellular antiviral
126 response, we performed an analysis of PBs and PB-regulated cytokine mRNAs after CoV
127 infection. Prior to this research, no published literature was available on human CoVs and PBs,
128 and only two previous reports mentioned PB dynamics after CoV infection. Murine hepatitis
129 virus (MHV) was reported to increase PBs at early infection times, while transmissible
130 gastroenteritis coronavirus (TGEV) infected cells displayed complete PB loss by 16 hours post

131 infection [86,87]. Observations that SARS-CoV-2 infection induced elevated levels of many PB-
132 regulated cytokines, such as IL-6, IL-10, IL-1β and TNF [53,54,57,69,70] suggested that human
133 CoVs like SARS-CoV-2 may reshape the cellular innate immune response in part by targeting
134 PBs for disassembly. We now present the first evidence to show that three human CoVs,
135 including SARS-CoV-2 trigger PB disassembly during infection. By screening a SARS-CoV-2
136 gene library, we identified that the nucleocapsid (N) protein was sufficient for PB disassembly.
137 However, this feature is not common for all human coronavirus N proteins, as overexpression of
138 MERS-CoV-N, OC43-N, 229E-N and NL63-N was insufficient to induce PB loss. SARS-CoV-
139 2 N protein expression was also sufficient to increase levels of inflammatory transcripts known
140 to be elevated in SARS-CoV-2 infection: IL-6 and TNF. Taken together, these results show that
141 PBs are targeted for disassembly by human CoV infection, and that this phenotype may
142 contribute to reshaping cytokine responses to SARS-CoV-2 infection.

143 **Results**

144 Infection with human coronaviruses causes PB loss

145 Endothelial cells (ECs) have emerged as playing a significant role in severe COVID; as sentinel
146 immune cells they are important sources for many of the cytokines elevated in severe disease and
147 are infected by SARS-CoV-2 *in vivo* [56,58-60,88]. However, others have shown that
148 commercial primary human umbilical vein endothelial cells (HUVECs) require ectopic
149 expression of the viral receptor, ACE2, to be susceptible to SARS-CoV-2 [89]. We recapitulated
150 those findings and showed that after HUVECs were transduced with an ACE2-expressing
151 lentivirus ($HUVEC^{ACE2}$), they were permissive for SARS-CoV-2 (Fig 1A). To use $HUVEC^{ACE2}$
152 for studies on PB dynamics, we confirmed that ACE2 ectopic expression had no effect on PB
153 number in HUVECs (Fig S1). Confirming this, we infected $HUVEC^{ACE2}$ with SARS-CoV-2 to
154 determine if PBs were altered. SARS-CoV-2 infected cells were identified by immunostaining
155 for the viral nucleocapsid (N) while PBs were identified by immunostaining for two different PB
156 resident proteins, the RNA helicase DDX6, and the decapping cofactor, Hedls. PBs, measured by
157 staining for both markers, were absent in most SARS-CoV-2 infected $HUVECs^{ACE2}$ by 24 hours
158 post infection (Fig 1B-E). We quantified the loss of cytoplasmic puncta using a method
159 described previously [90] and showed that by 24 hours post infection, SARS-CoV-2 infected
160 cells displayed a significant reduction in PBs compared to mock-infected controls (Fig 1C, E).
161

162 To confirm that PBs were reduced by SARS-CoV-2 infection of naturally permissive cells
163 derived from respiratory epithelium, we infected Calu-3 cells with SARS-CoV-2. Infected cells
164 were identified by immunostaining for N protein 48 hours after infection and PBs were stained
165 for DDX6. We observed PB loss in most but not all infected cells (Fig 1F). PB loss was more

166 often associated with cells that displayed N-positive staining throughout the cytoplasm or N-
167 positive multinucleated syncytial cells and was less frequent in cells that had not yet fused or
168 displayed punctate N protein staining (Fig 1F). Our attempts to quantify PB loss in infected
169 Calu-3 were not successful because cell clumping and crowding displayed by these cells made it
170 difficult for our CellProfiler pipeline to identify discrete infected cells.
171
172 To determine if PBs were lost in response to infection with other human coronaviruses, we
173 established infection models for the *Betacoronavirus*, OC43, and the *Alphacoronavirus*, 229E.
174 We found HUVECs were permissive to both OC43 and 229E (Fig 2A-B). We then performed a
175 time-course experiment wherein OC43-infected HUVECs were fixed at various times post
176 infection and immunostained for the viral N protein and the PB-resident protein DDX6. We
177 observed that PBs were largely absent in OC43 N protein-positive cells but present in mock-
178 infected control cells (Fig 2C-D). 229E-infected HUVECs were stained for DDX6 to measure
179 PBs and for dsRNA to denote infected cells due to a lack of commercially available antibodies
180 for 229E. CoV infected cells are known to form an abundance of dsRNA due to viral replication
181 and transcription from a positive-sense RNA genome making this a suitable marker for viral
182 infection [91]. After 229E infection, we also found that PBs were significantly reduced (Fig 2D-
183 E).
184
185 PBs will disassemble if key scaffolding proteins are lost; these include the RNA helicase DDX6,
186 the translation suppressor 4E-T, the decapping cofactors Hedls/EDC4 and DCP1A, and the
187 scaffolding molecule Lsm14A [92]. To elucidate if CoV-infected cells displayed decreased
188 steady-state levels of PB resident proteins, we immunoblotted infected cell lysates for PB

189 proteins XRN1, DCP1A, or DDX6, and Hedls (Fig 3). SARS-CoV-2 infection of HUVEC^{ACE2}
190 cells did not alter steady-state protein levels of these proteins compared to uninfected cells (Fig
191 3A). OC43-infected HUVECs displayed comparable levels of XRN1, DCP1A, and Hedls
192 relative to uninfected cells; however, OC43 infection decreased steady-state levels of DDX6 at
193 both 12 and 24 hpi (Fig 3B). 229E-infected HUVECs showed no detectible change in PB protein
194 expression after infection compared to controls (Fig 3C).
195
196 PBs are important sites for the post-transcriptional control of inflammatory cytokine transcripts
197 containing AU-rich elements, and PB loss correlates with enhanced levels of some of these
198 transcripts [7,12-15]. To determine if ARE-mRNAs are elevated, and therefore subject to
199 regulation during CoV infection, we harvested total RNA from SARS-CoV-2-, OC43- or 229E-
200 infected HUVECs and performed RT-qPCR for five ARE-containing cytokine transcripts, IL-6,
201 CXCL8, COX-2, GM-CSF, and IL-1β (Fig 4A-C). We observed increased levels of three of
202 these transcripts, IL-6, CXCL8, and COX-2, compared to uninfected cells, particularly in SARS-
203 CoV-2 infected cells (Fig 4A). Taken together, these data indicate that infection with human
204 coronaviruses including SARS-CoV-2 induces PB loss, and that some PB-regulated cytokine
205 ARE-mRNAs are elevated during CoV infection.
206
207 <u>A screen of SARS-CoV-2 genes reveals mediators of PB loss</u>
208 The genome of SARS-CoV-2 is predicted to contain up to 14 open reading frames (ORFs). The
209 two N-terminal ORFs (1a and 1ab) encode two large polyproteins which are processed by viral
210 proteases into 16 non-structural proteins (nsp1-16) essential for viral genome replication and
211 transcription [46]. The 3' end of the SARS-CoV-2 genome is predicted to code for ORFs that are

212 expressed from 9 subgenomic mRNAs [93]. Among these are the four structural proteins spike
213 (S), envelope (E), membrane (M) and nucleocapsid (N) and up to 9 potential accessory proteins,
214 not all of which have been validated as expressed in infected cells [93]. To test which SARS-
215 CoV-2 gene product(s) was responsible for PB disassembly, we obtained a plasmid library of 27
216 SARS-CoV-2 genes from the Krogan lab; this library included 14 nsps (excluding nsp3 and
217 nsp16), all structural (S, E, M, N) and candidate accessory genes (ORFs 3a, 3b, 6, 7a, 7b, 8, 9b,
218 9c, 10) [93]. We individually transfected each plasmid and immunostained for each of the
219 SARS-CoV-2 proteins using antibodies to the Strep-tag II and for PBs using anti-DDX6 (Fig
220 5A). Relative to control cells, many SARS-CoV-2 ORF transfected cells still displayed DDX6-
221 positive PBs; however, expression of some SARS-CoV-2 genes reduced DDX6-positive puncta,
222 including N and ORF7b (Fig 5A). We quantified the number of DDX6-positive PBs per cell for
223 each transfection as in [90] and found that the average number of PBs per cell was reduced
224 relative to our negative control after transfection of eight SARS-CoV-2 genes: nsp7, ORF7b, N,
225 ORF9b, ORF3b, nsp6, nsp1, and nsp11 (Fig 5B-C). This quantification was performed in two
226 different ways. In most cases, transfected cells were identified by co-staining for the Strep-tag II
227 fused to each gene, as shown for N, E and ORF7b (Fig 5A). In such cases, we quantified DDX6-
228 positive puncta only in those cells that were transfected and not in bystander cells (Fig 5B,
229 thresholded). These data identified three SARS-CoV-2 proteins that may cause PB loss in a cell
230 autonomous manner: nsp7, ORF7b and N (Fig 5B). For the remaining transfections (nsp1, nsp5,
231 nsp6, nsp11, nsp13, nsp14, ORF3b, ORF6, ORF9b, ORF9c) immunostaining for the Strep-tag II
232 was not robust and we were unable to threshold our PB counts. In these samples, we quantified
233 PBs in all cells of the monolayer (Fig 5C, unthresholded). These data identified five additional
234 SARS-CoV-2 proteins from our screen that may cause PB loss: ORF9b, ORF3b, nsp1, nsp6 and

235 nsp11 (Fig 5C). We verified the expression of all constructs, including low expressors (nsp1,
236 nsp5, nsp6, nsp11, nsp13, nsp14, ORF3b, ORF6, ORF9b and ORF9c) by immunoblotting whole
237 cell lysates harvested from parallel transfections (Fig 5D). We were unable to detect nsp4 by
238 immunoblotting; however, we did visualize this protein by immunostaining (Fig 5D). We
239 eliminated low confidence hits (nsp7, ORF9b) and low expressors (nsp6, nsp11) from further
240 studies and proceeded with validation of the top four hits (ORF7b, N, ORF3b, nsp1).
241
242 The nucleocapsid protein of SARS-CoV-2 induces PB disassembly
243 We tested four top hits from our PB screen in more relevant endothelial cells as these cells can
244 be infected, express inflammatory cytokines, and stain robustly for PBs. HUVECs were
245 transduced with recombinant lentiviruses expressing N, nsp1, ORF3b, and ORF7b or empty
246 vector control lentiviruses. We also included recombinant lentiviruses expressing nsp14 in this
247 experiment because of its exoribonuclease activity and ability to diminish cellular translation and
248 interferon responses [84]. Transduced cells were selected for transgene expression and then fixed
249 and stained for the endogenous PB marker protein DDX6 and for the Strep-tag II on each of
250 SARS-CoV-2 constructs. We observed robust staining of the viral nucleocapsid (N) protein in
251 the transduced cell population (Fig 6A) but were unable to detect expression of nsp1, nsp14,
252 ORF3b or ORF7b by immunostaining (Fig S2A). We quantified PB loss in the selected cells and
253 observed decreased PB numbers in cell populations expressing N, nsp1, nsp14, ORF3b and
254 ORF7b; however, the most robust PB loss was induced in N-expressing cells, which displayed a
255 five-fold reduction in PB numbers as well as strong immunostaining (Fig 6B, Fig S2). We were
256 concerned that we could not detect the other four transgenes by immunostaining; therefore, we
257 performed immunoblotting for the Strep-II tag on lysates from each transduced cell population

258 (Fig S2C). Although we detected a strong band of ~50 kDa at the predicted molecular weight for
259 N, we were unable to detect bands for nsp14, ORF3b and ORF7b, while the most prominent
260 band for nsp1 did not migrate at the predicted molecular weight of ~20 kDa (Fig S2) [94,95]. For
261 these reasons, we decided to focus the remainder of our analysis on the N protein.
262
263 As PBs are dynamic RNP granules that undergo transient disassembly and assembly, we wanted
264 to determine whether N-mediated PB loss was caused by enhanced disassembly of PBs or the
265 prevention of their *de novo* assembly. To determine this, we treated N-expressing HUVECs with
266 sodium arsenite, a known inducer of PB assembly. Consistent with our previous observation, PB
267 loss was observed post N expression in our untreated control (Fig 6C-F). However, in N-
268 expressing cells that were treated with sodium arsenite, robust PB expression was still observed
269 (Fig 6C-F). PBs were immunostained using two different PB resident proteins, DDX6 and Hedls.
270 These data showed that N expression is sufficient to cause PB loss, and that the absence of PBs
271 in N-expressing cells is a result of enhanced PB disassembly.
272
273 We showed that human CoVs OC43 and 229E also cause PB loss during infection (Fig 2);
274 therefore, we were interested to determine if ectopic expression of nucleocapsid proteins from
275 these or other human CoVs were sufficient to mediate PB disassembly. To test this, we
276 transduced HUVECs with recombinant lentiviruses expressing the N protein from SARS-CoV-2
277 as well as N derived from two other Betacoronaviruses, MERS-CoV N-Flag and OC43 N.
278 Expression of MERS-CoV and OC43 N proteins did not lead to significant PB loss compared to
279 SARS-CoV-2-N (Fig 7A-B). We also tested two N proteins from human Alphacoronaviruses,
280 229E N-Flag and NL63 N-Flag and found that neither of these induced significant PB loss

281 compared to SARS-CoV-2 N (Fig 7C-D). Consistent with this, immunoblotting of steady state
282 levels of PB resident proteins after N protein overexpression showed that most PB proteins tested
283 remained unchanged in the context of ectopic expression (Fig 7E-F). The exception to this was
284 the decapping factor, Hedls/EDC4, which was slightly decreased after expression of SARS-CoV-
285 2 N, but slightly increased after expression of the four other N genes tested (Fig 7E-F). The
286 significance of this observation is not yet clear.
287
288 To understand if PB disassembly correlated with changes to PB-regulated inflammatory cytokine
289 transcripts, we performed RT-qPCR for the three AU-rich containing mRNAs, IL-6, CXCL8 and
290 TNF that were elevated after infection with SARS-CoV-2, OC43 and 229E (Fig 4). PBs control
291 cytokine transcript levels post-transcriptionally because they modulate mRNA decay; however,
292 in uninduced ECs, the transcription of these mRNAs is minimal. For example, TNF mRNA
293 could not be readily detected by RT-qPCR without transcriptional activation. Therefore, we
294 treated control and N-expressing HUVECs with TNF to activate cytokine transcription and then
295 assessed if N protein expression enhanced cytokine mRNA level post-transcriptionally. In the
296 absence of TNF, no significant change of mRNA abundance was observed for any of the
297 coronaviruses N proteins tested (Fig 8A-C, 0 hour no treatment). Ectopic expression of SARS-
298 CoV-2-N enhanced transcript levels of IL-6, CXCL8, and TNF 24 hours after transcription was
299 induced (Fig 8A-C). However, we did not observe enhanced transcript levels after expression of
300 N protein from MERS-CoV, OC43, 229E, or NL63 (Fig 8A-C), consistent with earlier
301 observations that their expression does not induce PB loss.
302

303 Taken together, we present the novel finding that three human CoVs induce PB loss and that for
304 SARS-CoV-2, the nucleocapsid protein is responsible for this loss. Moreover, we tested four
305 other CoV N proteins and found that of these, only SARS-CoV-2 N was sufficient to induce PB
306 disassembly and concomitantly enhance levels of selected AU-rich element-containing cytokine
307 mRNAs.
308

309 **Discussion**

310 In this manuscript, we present the first evidence to show that human CoVs, including SARS-
311 CoV-2, induce PB loss after infection. PBs are fundamental sites of post-transcriptional control
312 of gene expression and are particularly relevant to the regulation of cytokine production. Our
313 major findings are as follows. i) Three human coronaviruses, SARS-CoV-2, OC43, and 229E
314 induced PB loss. ii) The SARS-CoV-2 nucleocapsid (N) protein was sufficient to cause PB loss
315 and N protein expression elevated levels of PB-regulated cytokine transcripts encoding IL-6 and
316 TNF. Taken together, these data point to PB loss as a central feature of CoV infection.
317 Moreover, because viral induced PB disassembly elevates PB-regulated cytokine transcripts, this
318 phenotype may contribute to the uncontrolled expression of proinflammatory molecules
319 observed in severe SARS-CoV-2 infection.

320

321 We screened 27 SARS-CoV-2 gene products by transfection in HeLa cells [93] and initially
322 identified eight candidate genes that reduced PB numbers (Fig 5). Validation of a subset of these
323 in HUVECs revealed that the most robust and consistent mediator of PB loss was the SARS-
324 CoV-2 viral N protein (Fig 6). The N protein is the most abundant produced protein during CoV
325 replication [96]. The SARS-CoV-2 N protein is 419 amino acids long and has two globular and
326 three intrinsically disordered protein domains, including a central disordered serine-arginine
327 (SR-rich) linker region [96-98]. The N protein is a multifunctional RNA-binding protein (RBP)
328 essential for viral replication; it coats the viral genome and promotes viral particle assembly
329 [46,98-101]. Several recent reports have shown that N protein undergoes liquid-liquid phase
330 separation with RNA, an event which may be regulated by phosphorylation of multiple serine
331 residues in the SR-region and is an important feature of viral assembly[101-106]. The N protein

332 is also an important modulator of antiviral responses [85,107,108]. A recent study showed that
333 low doses of N protein supressed the production of IFN and some PB-regulated inflammatory
334 cytokines, while high doses of N protein promoted their production [85]. These observations are
335 consistent with our phenotype of PB disassembly, which correlates with later infection times,
336 high expression of N protein and immunofluorescent staining throughout the cytoplasm (Fig 1,
337 Fig 6).
338
339 We subsequently screened four other coronavirus N proteins from OC43, MERS, 229E and
340 NL63, and discovered that the phenotype of N-mediated PB disassembly was not conserved
341 among N proteins but was unique to SARS-CoV-2-N (Fig 7). Despite conservation of motifs, the
342 N proteins from different human CoVs possess low sequence conservation at the amino acid
343 level (~50%) and have been reported to exhibit different properties [109]. One key difference
344 that we observed by immunoblotting was the presence of a lower molecular weight ~37 kDa
345 band recognized by our anti-N antibody for SARS-CoV-2. We did not observe the 37kDa N
346 product after OC43 infection, transduction with OC43 N protein or transduction with C-
347 terminally Flag-tagged N proteins from 229E, NL63, or MERS-CoV (Fig 2, Fig 7C). Steady
348 state levels of the ~37 kDa product increased over the course of SARS-CoV-2 infection,
349 consistent with the timing of PB disassembly. Other groups have noted that the SARS-CoV-2
350 variant of concern (VOC), Alpha (B.1.1.7), produces an additional subgenomic mRNA from
351 which a truncated version of N, termed N*, can be produced [68,110,111]. Translation of the N*
352 ORF is predicted to start at an internal in-frame methionine residue (Met210) within the N
353 protein [110,111] . Alignment of the SARS-CoV-2 N protein sequence against other N proteins
354 revealed that of the human CoVs, only SARS-CoV-1 and SARS-CoV-2 N retained a methionine

355 at position 210 (229E: NC_002645.1, HKU1: NC_006577.2, MERS: NC_019843.3, NL63:
356 NC_005831.2, OC43: NC_006213.1, SARS-1: NC_004718.3, SARS-2: NC_045512.2). Viruses
357 often capitalize on downstream methionine residues to translate truncated protein products with
358 subcellular localization or functions that differ from their full-length counterparts as a clever way
359 to increase coding capacity [112,113]. Our ongoing investigation of the precise nature of the
360 SARS-CoV-2 N protein truncation product we observe during infection and overexpression may
361 reveal that it has a specific role in PB disassembly.
362
363 The PB protein MOV10, and other components of RNA processing machinery, were revealed as
364 potential interactors with the N protein [114]; however, we do not observe colocalization of N
365 protein with PBs after immunofluorescent staining of SARS-CoV-2 infected cells or N-
366 expressing cells. Based on our data, we consider two possible mechanisms of N protein mediated
367 PB disassembly. First, N protein may mediate PB disassembly by phase separation with a PB
368 protein(s). This is similar to what has already been shown for N-mediated disruption of
369 cytoplasmic stress granules, important cytoplasmic biomolecular condensates that correlate with
370 cellular translational shutdown [35]. N protein localizes to stress granules and binds the essential
371 protein, G3BP1, preventing its interaction with other stress granule proteins and blocking stress
372 granule formation [115-117]. Although the precise domain required for this effect has been
373 debated, more than one report suggests that the N-terminal intrinsically disordered region is
374 required for stress granule disruption [116,118]. Second, a possible reason for PB loss may be
375 the indiscriminate binding of RNA by N protein. N protein could be acting as sponge for RNA,
376 pulling it out of cytoplasm, thereby reducing the RNA-protein interactions required for phase
377 separation of PBs [24,115]. We are currently engaged in site-directed and truncation mutagenesis

378 studies to determine the precise region(s) of SARS-CoV-2- N that is essential for PB
379 disassembly.
380
381 Prior to this report, little was known about CoVs and PBs, and the information that was
382 published was contradictory. Infection with murine hepatitis virus (MHV) was reported to
383 increase PBs, whereas transmissible gastroenteritis coronavirus (TGEV) decreased PBs [86,87].
384 Since the initiation of our study, one additional publication used ectopic expression of one of the
385 SARS-CoV-2 CoV proteases, nsp5, to test if it was capable of PB disassembly. Consistent with
386 the results of our screen (Fig 5), nsp5 did not mediate PB loss [32]. In this manuscript, we now
387 confirm that SARS-CoV-2, OC43, and 229E induce PB disassembly (Fig 1, Fig 2) [34]. We also
388 observed that different human CoVs cause PB loss using different viral gene products; SARS-
389 CoV-2 utilizes N protein but OC43 and 229E do not, a diversity which further underscores that
390 PB disassembly by viruses is intentional and not incidental. Because PBs are composed of
391 numerous cellular molecules with established (e.g. APOBEC, MOV10) or potential (decapping
392 enzymes and exonucleases that could degrade viral RNA) antiviral activities, it is possible that
393 viruses may target PBs for disassembly to negate their antiviral activity [28,29,31,39-45,119]. A
394 recent screen for cellular proteins that bind SARS-CoV-2 viral RNA captured two PB proteins
395 (Lsm14a and MOV10), which suggests CoV RNA may be shuttled to PBs [120]. That said, our
396 evidence does not yet discern if the proposed antiviral role of PB-localized enzymes is promoted
397 by phase separation of molecules into PBs or not; if so, we would predict that the antiviral
398 function of these molecules is lost when PB granules decondense. Emerging evidence suggests
399 that activity of the decapping enzymatic complex is increased by phase separation and decreased
400 in solution [9,24,121]. Thus, we speculate that PBs are direct-acting antiviral granules that can

401 restrict virus infection when present as visible condensates; for this reason, they are targeted for
402 disassembly by most viruses.
403
404 One possibility is that PBs are antiviral because their proteins help the cell respond to signals that
405 activate innate immune pathways [28,30,122,123]. In support of this, TRAF6 was shown to
406 control Dcp1a localization to PBs using ubiquitylation, suggesting that antiviral signaling is
407 more complex than previously appreciated and integrates transcriptional responses with cytokine
408 mRNA suppression in PBs [122,124]. Moreover, the PB protein Lsm14A has been shown to
409 bind to viral RNA/DNA after infection-induced PB disassembly to promote IRF3 activation and
410 IFN-β production [123]. Although it remains unclear if the higher order condensation of many
411 proteins into the PB regulates their proposed antiviral activity, what is clear is that the outcome
412 of PB disassembly is a reversal of the constitutive decay or translational suppression of cytokine
413 mRNAs that would normally occur there [7,12-15,125]. We speculate that when viruses
414 coordinate an attack to cause PB loss, this event is viewed as a danger signal by the cell: it
415 relieves cytokine mRNA suppression and increases the production of proinflammatory cytokines
416 to act as a call for reinforcements. In this way, PB disassembly is connected to the innate
417 immune response and is one of many signals that notify the immune system that a cell is
418 infected. In situations where interferon responses are delayed or defective, as is emerging for
419 SARS-CoV-2 and severe COVID-19 [65-67], PB disassembly may occur to alert the immune
420 system of an infection, and may be an important contributing factor to pathogenic cytokine
421 responses. Ongoing work in our laboratory continues to explore this model of PB regulation of
422 virus infection.
423

424 In summary, our work adds to a growing body of literature highlighting that many viruses target
425 PBs for disassembly using diverse mechanisms, supporting the idea that PBs restrict viral
426 infection. We showed that the N protein of SARS-CoV-2 is sufficient for PB disassembly and
427 this phenotype correlated with elevated levels of PB-regulated cytokine transcripts encoding IL-6
428 and TNF. This is significant, as we know that SARS-CoV2 infection is characterized by elevated
429 expression of both these cytokines [53]. Not only does this work describe a previously
430 uncharacterized cellular target of CoV infection, but we have identified a novel mechanism
431 which may contribute to the dysregulated cytokine response exhibited by severe SARS-CoV-2
432 infection.
433
434
435

436 **Materials and Methods**

437 **Cell Culture and Drug Treatments**

438 All cells were maintained in humidified 37 °C incubators with 5% CO_2 and 20% O_2. Vero E6
439 (ATCC), HEK293T cells (ATCC), HeLa Tet-Off cells (Clontech) and HeLa Flp-In TREx GFP-
440 Dcp1a cells (a generous gift from Anne-Claude Gingras) were cultured in DMEM (Thermo
441 Fisher) supplemented with 100 U/mL penicillin, 100 µg/mL streptomycin, 2 mM L-glutamine
442 (Thermo Fisher) and 10% FBS (Thermo Fisher). Calu3 (ATCC) and MRC-5 cells (ATCC) were
443 cultured in EMEM (ATCC) supplemented with 100 U/mL penicillin, 100 µg/mL streptomycin, 2
444 mM L-glutamine and 10% FBS. HUVECs (Lonza) were cultured in endothelial cell growth
445 medium (EGM-2) (Lonza). HUVECs were seeded onto tissue culture plates or glass coverslips
446 coated with 0.1 % (w/v) porcine gelatin (Sigma) in 1x PBS. For sodium arsenite treatment,
447 HUVECs were treated with 0.25 mM sodium arsenite (Sigma) or a vehicle control for 30 min.

448 **Plasmids and Cloning**

449 pLenti-IRES-Puro SARS-CoV-2 plasmids were a generous gift from the Krogan Lab [93].
450 pLJM1-OC43-N was cloned from pGBW-m4134906, a gift from Ginkgo Bioworks & Benjie
451 Chen (Addgene plasmid #151960; http://n2t.net/addgene:151960; RRID:Addgene_151960)
452 using BamHI and EcoRI restriction sites (NEB). pLJM1-NL63-N-FLAG was cloned from
453 pGBW-m4134910, a gift from Ginkgo Bioworks & Benjie Chen (Addgene plasmid #151939;
454 http://n2t.net/addgene:151939; RRID:Addgene_151939) using BamHI and EcoRI. pLJM1-229E-
455 N-FLAG was cloned from pGBW-m4134902, a gift from Ginkgo Bioworks & Benjie Chen
456 (Addgene plasmid #151912; http://n2t.net/addgene:151912; RRID:Addgene_151912) using
457 BamHI and EcoRI. pLJM1-MERS-CoV-N-FLAG was cloned from SinoBiological (cat
458 #VG40068-CF) using BamHI and EcoRI (Table 1).

459 **Transient Transfections**

460 Transient transfections were performed using Fugene (Promega) according to manufacturer's
461 guidelines. Briefly, HeLa Flp-In TREx GFP-Dcp1a cells were seeded in 12-well plates at
462 150,000 cells/well in antibiotic-free DMEM. Cells were transfected with 1 µg of DNA and 3 µL
463 of Fugene for 48 hours before processing.

464 **Production and use of Recombinant Lentiviruses**

465 All recombinant lentiviruses were generated using a second-generation system. HEK293T cells
466 were transfected with psPAX2, MD2-G, and the lentiviral transfer plasmid containing a gene of
467 interest using polyethylimine (PEI, Polysciences). 6 hours after transfection, serum-free media
468 was replaced with DMEM containing serum but no antibiotics. Viral supernatants were
469 harvested 48 hours post-transfection and frozen at -80°C until use. For transduction, lentiviruses
470 were thawed at 37°C and added to target cells in complete media containing 5 µg/mL polybrene
471 (Sigma). After 24 hours, the media was replaced with selection media containing 1 µg/mL
472 puromycin or 5 µg/mL blasticidin (ThermoFisher) and cells were selected for 48 h before
473 proceeding with experiments.

474 **Immunofluorescence**

475 Cells were seeded onto 18mm round, #1.5 coverslips (Electron Microscopy Sciences) for
476 immunofluorescence experiments. Following treatment, cells were fixed for 10 or 30 (if infected
477 with SARS-CoV-2) min in 4% (v/v) paraformaldehyde (Electron Microscopy Sciences).
478 Samples were permeabilized with 0.1% (v/v) Triton X-100 (Sigma-Aldrich) for 10 min at room
479 temperature and blocked in 1% human AB serum (Sigma-Aldrich) in 1X PBS 1 h at room
480 temperature. Primary and secondary antibodies (Table 2) were diluted in 1% human AB serum
481 and used at the concentrations in Table 2. Nuclei were stained with 1 µg/ml Hoechst

482 (Invitrogen). Samples were mounted with Prolong Gold AntiFade mounting media
483 (ThermoFisher).

484 **Immunoblotting**

485 Cells were lysed in 2X Laemmli buffer and stored at -20°C until use. The DC Protein Assay
486 (Bio-Rad) was used to quantify protein concentration as per the manufacturer's instructions. 10-
487 15 µg of protein lysate was resolved by SDS-PAGE on TGX Stain-Free acrylamide gels
488 (BioRad). Total protein images were acquired from the PVDF membranes after transfer on the
489 ChemiDoc Touch Imaging system (BioRad). Membranes were blocked in 5% BSA in TBS-T
490 (Tris-buffered saline 0.1% Tween-20). Primary and secondary antibodies were diluted in 2.5%
491 BSA, dilutions can be found in Table 2. Membranes were visualized using Clarity Western ECL
492 substrate and the ChemiDoc Touch Imaging system (BioRad).

493 **Quantitative PCR**

494 RNA was collected using the RNeasy Plus Mini Kit (Qiagen) according to the manufacturer's
495 instructions and stored at -80°C until further use. RNA concentration was determined using
496 NanoDrop One^{C} (ThermoFisher) and 500 ng of RNA was reverse transcribed using qScript XLT
497 cDNA SuperMix (QuantaBio) using a combination of random hexamer and oligo dT primers,
498 according to the manufacturer's instructions. Depending on starting concentration, cDNA was
499 diluted between 1:10 and 1:20 for qPCR experiments and SsoFast EvaGreen Mastermix (Biorad)
500 was used to amplify cDNA. The ΔΔquantitation cycle (Cq) method was used to determine the
501 fold change in expression of target transcripts. qPCR primer sequences can be found in Table 3.

502 **Virus Propagation**

503 Experiments with SARS-CoV-2 were conducted in a containment level-3 (CL3) facility, and all
504 standard operating procedures were approved by the CL3 Oversight Committee and Biosafety

505 Office at the University of Calgary. Stocks of SARS-CoV-2 Toronto-01 isolate [126] were
506 propagated in Vero E6 cells. To produce viral stocks, Vero E6 cells were infected at an MOI of
507 0.01 for 1 hour in serum-free DMEM at 37˚C. Following adsorption, DMEM supplemented with
508 2% heat inactivated FBS and 100 U/mL penicillin/streptomycin/glutamine was added to the
509 infected wells. 24-48 days post-infection (dpi), the supernatant was harvested and centrifuged at
510 500 x *g* for 5 min to remove cellular debris. Virus stocks were aliquoted and stored at -80˚C for
511 single use. SARS-CoV-2 titres were enumerated using plaque assays on Vero E6 cells as
512 previously described [127]using equal parts 2.4% w/v semi-solid colloidal cellulose overlay
513 (Sigma; prepared in ddH_2O) and 2X DMEM (Wisent) with 1% heat inactivated FBS and 1%
514 PSQ.
515 Experiments with hCoV-OC43 (ATCC VR-1558) and hCoV-229E (ATCC VR-740) were
516 conducted in under containment level-2 conditions. hCoV-OC43 and hCoV-229E were
517 propagated in Vero E6 and MRC-5 cells, respectively. Cells were infected at an MOI of 0.01 for
518 1 hour in serum-free media at 33˚C. Following adsorption, the viral inoculum was removed and
519 replaced with fresh media supplemented with 2% heat inactivated FBS and 100 U/mL
520 penicillin/streptomycin/glutamine. After 5-6 dpi, the supernatant was harvested and cellular
521 debris was cleared by centrifugation. Virus stocks were aliquoted and stored at -80˚C. hCoV-
522 OC43 and hCoV-229E titres were enumerated using Reed and Muench tissue-culture infectious
523 dose 50% ($TCID_{50}$) in Vero E6 or MRC-5 cells, respectively.
524 **Virus Infection**
525 For experimental infections, cells were seeded into wells to achieve ~80% confluency at the time
526 of infection. The growth media was removed and replaced with 100 µL of viral inoculum diluted
527 in serum-free DMEM to reach the desired MOI and incubated at 37˚C for 1 hour, rocking the

528 plate every 10 min. Following incubation, the virus inoculum was removed and replaced with 1
529 mL of complete grown media.

530 **Processing Body Quantification**

531 Processing bodies were quantified using an unbiased image analysis pipeline generated in the
532 freeware CellProfiler (cellprofiler.org) [128] described in more detail in [90]. First, nuclear
533 staining was used to identify individual cells applying a binary threshold and executing primary
534 object detection between 50 and 250 pixels. For each identified object (the nucleus), the
535 peripheral boundary of each cell was defined using the "Propagation" function. Using a
536 subtractive function to remove the nuclei from the total cell area, the cytoplasm of each cell was
537 defined. The cytoplasm area mask was then applied to the matched image stained for PB proteins
538 (DDX6 or Hedls) to count only DDX6 or Hedls-positive cytoplasmic puncta. Only the
539 cytoplasms of "positive" staining cells (e.g. SARS-CoV-2 N protein channel) were quantified
540 unless otherwise indicated in corresponding figure legends. Background staining was reduced
541 using the "Enhance Speckles" function. Only DDX6 or Hedls-positive puncta with a defined size
542 and intensity range were quantified using "global thresholding with robust background
543 adjustments" function. All thresholds were consistent between experiments that used identical
544 staining parameters. For Figure 5, puncta counts were exported and RStudio was used for data
545 analysis.

546 **Statistics**

547 All statistical analyses were performed using GraphPad Prism 9.0. Significance was determined
548 using a paired Student's t-test unless otherwise indicated in corresponding figure legends.

549

550

551

552 **Table 1: Plasmids**

Plasmid	Use	Source	Mammalian Selection
pLJM1-Puro	Empty Vector Control	[90] [129]	Puromycin
pLJM1-BSD	Empty Vector Control	[129]	Blasticidin
pLJM1-ACE2	Overexpression		Blasticidin
pMD2.G	Lentivirus Generation	Addgene #12259	N/A
psPAX2	Lentivirus Generation	Addgene #12260	N/A
pLJM1-OC43-N	Overexpression	Addgene #151960	Puromycin
pLJM1-229E-N-FLAG	Overexpression	Addgene #151912	Puromycin
pLJM1-NL63-N-FLAG	Overexpression	Addgene #151939	Puromycin
pLJM1-MERS-CoV-N-FLAG	Overexpression	SinoBiological #VG40068-CF	Puromycin
pLenti-SARS-CoV-2-IRES-strep	Overexpression library	N Krogan (UCSF) [114]	Puromycin

553

554

555

556

557

558

559

560

561

562

563

564

565 **Table 2: Antibodies**

Antibody	Species	Vendor/Catalog #	Application	Dilution
Strep-Tag II	Mouse	Sigma (71590-M)	Immunofluorescence Immunoblot	1:1000 1:1000
DDX6	Rabbit	Bethyl (A300-461)	Immunofluorescence Immunoblot	1:1000 1:1000
Hedls	Mouse	Santa Cruz (sc-8418)	Immunofluorescence Immunoblot	1:1000 1:1000
Dcp1a	Rabbit	Novus (H00055802-M06)	Immunoblot	1:1000
Xrn1	Mouse	Abcam (ab231197)	Immunoblot	1:1000
Coronavirus OC43 Nucleocapsid	Mouse	Millipore (MAB-9012)	Immunofluorescence Immunoblot	1:500 1:1000
SARS-CoV2 Nucleocapsid	Rabbit	Novus (NBP3-05730)	Immunofluorescence	1:1000
SARS-CoV2 Nucleocapsid	Mouse	Novus (NBP3-05706)	Immunofluorescence Immunoblot	1:1000 1:1000
dsRNA clone J2	Mouse	Millipore (MABE-1134)	Immunofluorescence	1:100
FLAG	Mouse	CST (8146)	Immunofluorescence Immunoblot	1:1000 1:1000
Actin HRP-conjugated	Rabbit	CST (5215)	Immunoblot	1:10,000

566
567
568
569
570
571
572
573
574
575
576
577
578
579
580

581 **Table 3: qPCR primers**

Target	Direction	Sequence 5'→3'
HPRT	Forward	CTTTCCTTGGTCAGGCAGTATAA
HPRT	Reverse	AGTCTGGCTTATATCCAACACTTC
18S	Forward	TTCGAACGTCTGCCCTATCAA
18S	Reverse	GATGTGGTAGCCGTTTCTCAGG
IL6	Forward	GAAGCTCTATCTCGCCTCCA
IL6	Reverse	TTTTCTGCCAGTGCCTCTTT
CXCL8	Forward	AAATCTGGCAACCCTAGTCTG
CXCL8	Reverse	GTGAGGTAAGATGGTGGCTAAT
IL-1β	Forward	CTCTCACCTCTCCTACTCACTT
IL-1β	Reverse	TCAGAATGTGGGAGCGAATG
TNF	Forward	TCGAACCCCGAGTGACAA
TNF	Reverse	AGCTGCCCCTCAGCTTG
GM-CSF	Forward	AAATGTTTGACCTCCAGGAGCC
GM-CSF	Reverse	ATCTGGGTTGCACAGGAAGTT
COX-2	Forward	CCCTTGGGTGTCAAAGGTAA
COX-2	Reverse	GCCCTCGCTTATGATCTGTC

582

583

584 **Figure Legends**

585

586 **Figure 1. Processing bodies are absent in SARS-CoV-2 infected cells. A.** HUVECs were
587 transduced with recombinant lentiviruses expressing human ACE2, selected, and infected with
588 SARS-CoV-2 TO-1 isolate at an MOI of 3. At 6 or 24 hours post infection (hpi), virus-
589 containing supernatant was harvested and titered by $TCID_{50}$ assay. *n*=2. **B-E.** HUVEC-ACE2
590 cells were infected with SARS-CoV-2 (MOI = 3) or mock-infected. At 16 hpi or 24 hpi, cells
591 were fixed and immunostained for SARS-CoV-2 N protein (green) and either DDX6 (B, white)
592 or Hedls (D, white). Nuclei were stained with Hoechst (blue). DDX6 puncta (C) and Hedls
593 puncta (E) in mock or SARS-CoV-2-infected cells were quantified using CellProfiler and is
594 expressed as fold-change relative to mock. *n*=3; mean ± SD (*, $P < 0.05$; ***, $P < 0.001$). **G.**
595 Calu3 cells were infected with SARS-CoV-2 (MOI =2) or mock-infected. 48 hours later, cells
596 were fixed and immunostained for SARS-CoV-2 N (green), DDX6 (PBs; white). Nuclei were
597 stained with Hoechst (blue). Representative images from one of two independent experiments
598 are shown. *n*=2. Scale bar = 20 µm.

599 **Figure 2. Processing bodies are absent in OC43 and 229E infected cells. A-B.** Each well of
600 12-well plate of HUVECs were infected with OC43 ($TCID_{50} = 2 \times 10^4$) or 229E ($TCID_{50} = 2.4 \times$
601 10^3). Supernatants were harvested at 6, 12, and 24 hpi and titrated by $TCID_{50}$ on Vero E6 or
602 MRC5 cells for OC43 or 229E, respectively. *n*=2; mean ± SD. **C.** HUVECs were infected with
603 OC43 or mock-infected, fixed at 12 hpi or 24 hpi and immunostained for DDX6 (PBs; white)
604 and OC43 N protein (green). Nuclei were stained with Hoechst (blue) **D.** DDX6 puncta in mock
605 or OC43-infected cells were quantified as in Figure 1. *n*=3, mean ± SD (**, $P < 0.01$). **E.** Each
606 well of 12-well plate of HUVECs were infected with 229E ($TCID_{50} = 2.4 \times 10^3$) or mock-

607 infected, fixed at 6 hpi or 12 hpi and immunostained for DDX6 (white) or dsRNA (green).
608 Nuclei were stained with Hoechst (blue). **F.** DDX6 puncta in mock or 229E-infected cells as in
609 Figure 1. *n*=3; mean ± SD (*, P < 0.05; ns, nonsignificant). Scale bar = 20 µm.

610 **Figure 3. Coronavirus infection does not alter steady state levels of processing body**
611 **proteins. A.** HUVECs were transduced with human ACE2, selected, and infected with SARS-
612 CoV-2 at an MOI of 3. Cells were lysed at 6 and 12 hpi and immunoblotting was performed
613 using XRN1, Hedls, DCP1A, DDX6, SARS-Cov-2 N, and β-actin specific antibodies. One
614 representative experiment of three is shown. **B-C.** Each well of 12-well plate of HUVECs were
615 infected with OC43 (B, $TCID_{50} = 2 \times 10^4$) or 229E (C, $TCID_{50} = 2.4 \times 10^3$). Cells were lysed at
616 12 and 24hpi (B, OC43) or 6 and 12 hpi (C, 229E). Immunoblotting was performed using XRN1,
617 Hedls, DCP1A, DDX6, OC43 N protein (B only), and β-actin specific antibodies. One
618 representative experiment of three is shown.
619

620 **Figure 4. Steady state levels of selected ARE-mRNAs are elevated during coronavirus**
621 **infection. A.** HUVECs were transduced with recombinant lentiviruses expressing human ACE2,
622 selected, and infected with SARS-CoV-2 (MOI=3). RNA was harvested 24 hpi and RT-qPCR
623 was performed using IL-6, CXCL8, COX-2, GM-CSF, IL-1β and HPRT specific primers. Values
624 are represented as fold change relative to mock-infection. *n*=3; mean ± SD (*, P < 0.05; **, P <
625 0.01; ns, nonsignificant). **B-C.** HUVECs were infected with OC43 (B, $TCID_{50}/mL = 3.5 \times 10^4$)
626 or 229E (C, $TCID_{50}/mL = 1 \times 10^{3.24}$). RNA was harvested 24 and 12 hpi for OC43 (B) and 229E
627 (C), respectively, and RT-qPCR was performed as in (A). Values are represented as fold change
628 relative to mock-infection. *n*≥3; mean ± SD (*, P < 0.05; **, P < 0.01; ns, nonsignificant).
629

630 **Figure 5. Identification of SARS-CoV-2 ORFs that mediate processing body loss. A-C** HeLa
631 cells expressing GFP-Dcp1a were transfected with an empty vector or 2xStrep-tagged SARS-
632 CoV-2 ORFs for 48 hours then fixed and immunostained for Strep-tag (red) or DDX6 (white).
633 Nuclei were stained with Hoechst (blue). **A.** Select ORFs are shown; Scale bar = 20 µm. **B-C.**
634 DDX6 puncta were quantified using CellProfiler. In B, SARS-CoV-2 ORF-expressing cells were
635 thresholded by Strep-tag staining intensity. The intensity threshold used was defined as two
636 standard deviations above mean intensity in vector controls. Only DDX6 puncta in cells above
637 this threshold were counted. In C, transfected cells did not stain above this threshold; therefore,
638 DDX6 puncta in all cells were counted. Values are expressed as a fold-change difference
639 normalized to the vector control (hashed line). A one-way ANOVA with a Dunnett's post-hoc
640 analysis was performed, n=3; bars represent SEM; **=P<0.01. **D.** HeLa cells were transfected as
641 above for 48 hours and lysates were harvested in 2x Laemmli buffer. Samples were resolved by
642 SDS-PAGE on 4-15% gradient gels (BioRad) and immunoblotted with a Strep-Tag II antibody
643 (Sigma).
644
645 **Figure 6. Ectopic expression of SARS-CoV-2 N elicits processing body disassembly. A.**
646 HUVECs were transduced with recombinant lentiviruses ectopically expressing 2xStrep-tagged
647 SARS-CoV-2 N or controls and selected with puromycin for 48 hours. Samples were fixed and
648 immunostained for Strep-tag (green) and DDX6 (white). Nuclei were stained with Hoechst
649 (blue). Scale bar = 20 µm. **B.** DDX6 puncta were quantified per field of view using CellProfiler
650 as in Figure 1. Values are expressed as fold-change normalized to the control transduction; *n*=3;
651 mean ± SD (*, P < 0.05). **C-F.** HUVECs were transduced and selected as in A, then treated with
652 0.25 mM sodium arsenite or a vehicle control for 30 min, fixed and immunostained for either

653 Hedls (C, white) or DDX6 (D, white) and SARS-CoV-2 N (green). Nuclei were stained with
654 Hoechst (blue). Scale bar = 20 µm. Hedls puncta (D) and DDX6 puncta (F) were quantified per
655 field of view as in (B). *n*=2; mean ± SD.
656
657 **Figure 7. Processing body disassembly is not a common feature of all human coronavirus N**
658 **proteins. A.** HUVECs were transduced recombinant lentiviruses ectopically expressing N
659 protein from the betacoronaviruses MERS-CoV, OC43 or control lentiviruses. SARS-CoV-2 N
660 protein expressing lentiviruses were used as a positive control. Cells were selected, fixed and
661 immunostained for DDX6 (white) and either authentic N protein or a FLAG tag (green). Nuclei
662 were stained with Hoechst (blue). Scale bar = 20 µm. **B.** DDX6 puncta in EV or N-transduced
663 cells were quantified per field of view by CellProfiler and represented as fold-change relative to
664 EV-transduced cells. A one-way ANOVA with a Dunnett's post-hoc analysis was performed;
665 *n*=3; mean ± SD (**, P < 0.01; ns, nonsignificant). **C.** HUVECs were transduced with
666 recombinant lentiviruses ectopically expressing N protein from the alphacoronaviruses 229E,
667 NL63 or control lentiviruses. SARS-CoV-2 N protein expressing lentiviruses were used as a
668 positive control. Cells were fixed and immunostained as in (A). Scale bar = 20 µm. **D.** DDX6
669 puncta in EV or N-transduced cells were quantified per field of view by CellProfiler and
670 represented as fold-change relative to EV-transduced cells. A one-way ANOVA with a
671 Dunnett's post-hoc analysis was performed; *n*=3; mean ± SD (*, P < 0.05; ns, nonsignificant). **E-**
672 **F.** HUVECs were transduced as in A and C, respectively, harvested in 2x Laemmli buffer and
673 immunoblotting was performed using XRN1, Hedls, DCP1A, DDX6, N protein or FLAG, and β-
674 actin specific antibodies. One representative experiment of three is shown.
675

676 **Figure 8. Ectopic expression of SARS-CoV-2 N elevates selected ARE-mRNAs. A-C.**
677 HUVECs were transduced with recombinant lentiviruses ectopically expressing alpha- and
678 betacoronavirus N proteins or empty vector (EV) control, selected, and treated with 0.01 ng/L
679 soluble TNF to increase transcription of ARE-containing cellular mRNAs. Total RNA was
680 harvested at 0, 8, 12, and 24 hours post TNF treatment and RT-qPCR was performed using IL-6
681 (A), CXCL8 (B), TNF (C) and HPRT specific primers. Values are represented as fold-change
682 relative to EV-transduced cells for each time point. A one-way ANOVA with a Dunnett's post-
683 hoc analysis was performed; *n*=3; mean ± SD (*, $P < 0.05$).
684
685
686 **Supplemental Figure Legends**
687
688 **Figure S1. ACE2 expression does not alter processing body numbers. A-B**. HUVECs were
689 transduced with recombinant lentiviruses expressing human ACE2 or an empty vector (EV)
690 control, selected, fixed and immunostained for the PB-resident proteins Hedls (A) and DDX6
691 (B). Puncta were quantified using CellProfiler and normalized to control (EV) counts. *n*=2; mean
692 ± SD.
693
694 **Figure S2. Ectopic expression of four SARS-CoV-2 ORFs mediates processing body loss. A.**
695 HUVECs were transduced recombinant lentiviruses expressing 2xStrep-tagged SARS-CoV-2
696 nsp1, nsp14, ORF3b and ORF7b constructs or control lentiviruses and selected with puromycin
697 for 48 h. Samples were fixed and immunostained for Strep-tag (red) or DDX6 (white). Nuclei
698 were stained with Hoechst (blue). Scale bar = 20 μm. **B.** DDX6 puncta were quantified per field

699 of view using CellProfiler and expressed as a fold-change normalized to the empty vector

700 control; *n*=2; mean ± SD. **C**. HUVECs were transduced in (A). Lysates were harvested in 2x

701 Laemmli buffer. Samples were resolved by SDS-PAGE on 4-15% gradient gels (BioRad) and

702 immunoblotted with a Strep-Tag II antibody (Sigma).

703

704

705 **Acknowledgements**

706 We sincerely thank the members of the Corcoran lab for helpful discussions about this work. We
707 would like to thank Dr. Nevan Krogan (UCSF) for sharing the SARS-CoV-2 gene library. We
708 would like to thank Dr. Anne Vaahtokari of the Charbonneau Microscopy Facility for
709 microscopy support and Dr. Devender Kumar for CL3 facility support. MK was supported by a
710 CSM graduate training award, a CIHR CGS-M scholarship, and a CIHR doctoral award.
711 Operating funds to support this work derive from the Canadian Institutes of Health Research.
712 The Vaccine and Infectious Disease Organization (VIDO) receives operational funding for its
713 CL3 facility (InterVac) from the Canada Foundation for Innovation through the Major Science
714 Initiatives. VIDO also receives operational funding from the Government of Saskatchewan
715 through Innovation Saskatchewan and the Ministry of Agriculture.

716

717 **Author Contributions**

718 Mariel Kleer: Conceptualization, Experimentation, Analysis, Paper Writing
719 Rory P. Mulloy: Conceptualization, Experimentation, Analysis, Paper Writing
720 Carolyn-Ann Robinson: Conceptualization, Experimentation, Analysis, Paper Writing
721 Elizabeth L. Castle: Analysis
722 Maxwell Bui-Marinos: Experimentation, Paper Writing
723 Jennifer A. Corcoran: Conceptualization, Experimentation, Supervision, Funding Acquisition,
724 Project Administration, Paper Writing

725 **Conflict of Interest**

726 The authors have no competing interests to declare.

727

728 **References**

729 1. Eulalio A, Behm-Ansmant I, Schweizer D, Izaurralde E. P-body formation is a
730 consequence, not the cause, of RNA-mediated gene silencing. Mol Cell Biol. 2007;27:
731 3970–3981. doi:10.1128/MCB.00128-07

732 2. Eulalio A, Rehwinkel J, Stricker M, Huntzinger E, Yang S-F, Doerks T, et al. Target-
733 specific requirements for enhancers of decapping in miRNA-mediated gene silencing.
734 Genes Dev. Cold Spring Harbor Lab; 2007;21: 2558–2570. doi:10.1101/gad.443107

735 3. Hubstenberger A, Courel M, Bénard M, Souquere S, Ernoult-Lange M, Chouaib R, et al.
736 P-Body Purification Reveals the Condensation of Repressed mRNA Regulons. Mol Cell.
737 Elsevier Inc; 2017;68: 144–157.e5. doi:10.1016/j.molcel.2017.09.003

738 4. Youn J-Y, Dunham WH, Hong SJ, Knight JDR, Bashkurov M, Chen GI, et al. High-
739 Density Proximity Mapping Reveals the Subcellular Organization of mRNA-Associated
740 Granules and Bodies. Mol Cell. Elsevier Inc; 2018;69: 517–532.e11.
741 doi:10.1016/j.molcel.2017.12.020

742 5. Bakheet T, Hitti E, Khabar KSA. ARED-Plus: an updated and expanded database of
743 AU-rich element-containing mRNAs and pre-mRNAs. Nucleic Acids Research.
744 2018;46: D218–D220. doi:10.1093/nar/gkx975

745 6. Hitti E, Bakheet T, Al-Souhibani N, Moghrabi W, Al-Yahya S, Al-Ghamdi M, et al.
746 Systematic Analysis of AU-Rich Element Expression in Cancer Reveals Common
747 Functional Clusters Regulated by Key RNA-Binding Proteins. Cancer Res. 2016;76:
748 4068–4080. doi:10.1158/0008-5472.CAN-15-3110

749 7. Blanco FF, Sanduja S, Deane NG, Blackshear PJ, Dixon DA. Transforming growth
750 factor β regulates P-body formation through induction of the mRNA decay factor
751 tristetraprolin. Mol Cell Biol. 2014;34: 180–195. doi:10.1128/MCB.01020-13

752 8. Brengues M, Teixeira D, Parker R. Movement of eukaryotic mRNAs between
753 polysomes and cytoplasmic processing bodies. Science. American Association for the
754 Advancement of Science; 2005;310: 486–489. doi:10.1126/science.1115791

755 9. Riggs CL, Kedersha N, Ivanov P, Anderson P. Mammalian stress granules and P bodies
756 at a glance. J Cell Sci. 2020;133: jcs242487. doi:10.1242/jcs.242487

757 10. Khong A, Parker R. mRNP architecture in translating and stress conditions reveals an
758 ordered pathway of mRNP compaction. J Cell Biol. 2018;217: 4124–4140.
759 doi:10.1083/jcb.201806183

760 11. Matheny T, Rao BS, Parker R. Transcriptome-Wide Comparison of Stress Granules and
761 P-Bodies Reveals that Translation Plays a Major Role in RNA Partitioning. Mol Cell
762 Biol. 2019;39: 612. doi:10.1128/MCB.00313-19

763 12. Corcoran JA, Khaperskyy DA, Johnston BP, King CA, Cyr DP, Olsthoorn AV, et al.
764 Kaposi's sarcoma-associated herpesvirus G-protein-coupled receptor prevents AU-rich-
765 element-mediated mRNA decay. J Virol. 2012;86: 8859–8871. doi:10.1128/JVI.00597-
766 12

767 13. Corcoran JA, Johnston BP, McCormick C. Viral Activation of MK2-hsp27-
768 p115RhoGEF-RhoA Signaling Axis Causes Cytoskeletal Rearrangements, P-body
769 Disruption and ARE-mRNA Stabilization. Robertson ES, editor. PLoS Pathogens.
770 Public Library of Science; 2015;11: e1004597. doi:10.1371/journal.ppat.1004597

771 14. Franks TM, Lykke-Andersen J. TTP and BRF proteins nucleate processing body
772 formation to silence mRNAs with AU-rich elements. Genes Dev. 2007;21: 719–735.
773 doi:10.1101/gad.1494707

774 15. Vindry C, Marnef A, Broomhead H, Twyffels L, Ozgur S, Stoecklin G, et al. Dual RNA
775 Processing Roles of Pat1b via Cytoplasmic Lsm1-7 and Nuclear Lsm2-8 Complexes.
776 CellReports. 2017;20: 1187–1200. doi:10.1016/j.celrep.2017.06.091

777 16. Vandelli A, Cid Samper F, Torrent Burgas M, Sanchez de Groot N, Tartaglia GG. The
778 Interplay Between Disordered Regions in RNAs and Proteins Modulates Interactions
779 Within Stress Granules and Processing Bodies. J Mol Biol. 2021;: 167159.
780 doi:10.1016/j.jmb.2021.167159

781 17. Nosella ML, Forman-Kay JD. Phosphorylation-dependent regulation of messenger RNA
782 transcription, processing and translation within biomolecular condensates. Curr Opin
783 Cell Biol. 2021;69: 30–40. doi:10.1016/j.ceb.2020.12.007

784 18. Jalihal AP, Pitchiaya S, Xiao L, Bawa P, Jiang X, Bedi K, et al. Multivalent Proteins
785 Rapidly and Reversibly Phase-Separate upon Osmotic Cell Volume Change. Mol Cell.
786 2020;79: 978–990.e5. doi:10.1016/j.molcel.2020.08.004

787 19. Mitrea DM, Chandra B, Ferrolino MC, Gibbs EB, Tolbert M, White MR, et al. Methods
788 for Physical Characterization of Phase-Separated Bodies and Membrane-less Organelles.
789 J Mol Biol. 2018;430: 4773–4805. doi:10.1016/j.jmb.2018.07.006

790 20. Banani SF, Rice AM, Peeples WB, Lin Y, Jain S, Parker R, et al. Compositional Control
791 of Phase-Separated Cellular Bodies. Cell. 2016;166: 651–663.
792 doi:10.1016/j.cell.2016.06.010

793 21. Guillén-Boixet J, Kopach A, Holehouse AS, Wittmann S, Jahnel M, Schlüßler R, et al.
794 RNA-Induced Conformational Switching and Clustering of G3BP Drive Stress Granule
795 Assembly by Condensation. Cell. 2020;181: 346–361.e17.
796 doi:10.1016/j.cell.2020.03.049

797 22. Van Treeck B, Parker R. Emerging Roles for Intermolecular RNA-RNA Interactions in
798 RNP Assemblies. Cell. 2018;174: 791–802. doi:10.1016/j.cell.2018.07.023

799 23. Cougot N, Cavalier A, Thomas D, Gillet R. The dual organization of P-bodies revealed
800 by immunoelectron microscopy and electron tomography. J Mol Biol. 2012;420: 17–28.
801 doi:10.1016/j.jmb.2012.03.027

802 24. Corbet GA, Parker R. RNP Granule Formation: Lessons from P-Bodies and Stress
803 Granules. Cold Spring Harb Symp Quant Biol. 2019;84: 203–215.
804 doi:10.1101/sqb.2019.84.040329

805 25. Standart N, Weil D. P-Bodies: Cytosolic Droplets for Coordinated mRNA Storage.
806 Trends Genet. 2018;34: 612–626. doi:10.1016/j.tig.2018.05.005

807 26. Docena G, Rovedatti L, Kruidenier L, Fanning A, Leakey NAB, Knowles CH, et al.
808 Down-regulation of p38 mitogen-activated protein kinase activation and
809 proinflammatory cytokine production by mitogen-activated protein kinase inhibitors in
810 inflammatory bowel disease. Clin Exp Immunol. John Wiley & Sons, Ltd; 2010;162:
811 108–115. doi:10.1111/j.1365-2249.2010.04203.x

812 27. Jangra RK, Yi M, Lemon SM. DDX6 (Rck/p54) is required for efficient hepatitis C
813 virus replication but not for internal ribosome entry site-directed translation. J Virol.
814 2010;84: 6810–6824. doi:10.1128/JVI.00397-10

815 28. Ng CS, Kasumba DM, Fujita T, Luo H. Spatio-temporal characterization of the antiviral
816 activity of the XRN1-DCP1/2 aggregation against cytoplasmic RNA viruses to prevent
817 cell death. Cell Death & Differentiation. Nature Publishing Group; 2020;36: 932–20.
818 doi:10.1038/s41418-020-0509-0

819 29. Ostareck DH, Naarmann-de Vries IS, Ostareck-Lederer A. DDX6 and its orthologs as
820 modulators of cellular and viral RNA expression. Wiley Interdiscip Rev RNA. 2014;5:
821 659–678. doi:10.1002/wrna.1237

822 30. Dougherty JD, Tsai W-C, Lloyd RE. Multiple Poliovirus Proteins Repress Cytoplasmic
823 RNA Granules. Viruses. Multidisciplinary Digital Publishing Institute; 2015;7: 6127–
824 6140. doi:10.3390/v7122922

825 31. Dougherty JD, White JP, Lloyd RE. Poliovirus-mediated disruption of cytoplasmic
826 processing bodies. J Virol. 2011;85: 64–75. doi:10.1128/JVI.01657-10

827 32. Fan S, Xu Z, Liu P, Qin Y, Chen M. Enterovirus 71 2A Protease Inhibits P-Body
828 Formation To Promote Viral RNA Synthesis. J Virol. 2021;95: e0092221.
829 doi:10.1128/JVI.00922-21

830 33. Kanakamani S, Suresh PS, Venkatesh T. Regulation of processing bodies: From viruses
831 to cancer epigenetic machinery. Cell Biol Int. John Wiley & Sons, Ltd; 2021;45: 708–
832 719. doi:10.1002/cbin.11527

833 34. Gaete-Argel A, Márquez CL, Barriga GP, Soto-Rifo R, Valiente-Echeverría F.
834 Strategies for Success. Viral Infections and Membraneless Organelles. Front Cell Infect
835 Microbiol. 2019;9: 336. doi:10.3389/fcimb.2019.00336

836 35. McCormick C, Khaperskyy DA. Translation inhibition and stress granules in the
837 antiviral immune response. Nature Reviews Immunology. Nature Publishing Group;
838 2017;17: 647–660. doi:10.1038/nri.2017.63

839 36. Tsai W-C, Lloyd RE. Cytoplasmic RNA Granules and Viral Infection. Annu Rev Virol.
840 Annual Reviews; 2014;1: 147–170. doi:10.1146/annurev-virology-031413-085505

841 37. Onomoto K, Jogi M, Yoo J-S, Narita R, Morimoto S, Takemura A, et al. Critical role of
842 an antiviral stress granule containing RIG-I and PKR in viral detection and innate
843 immunity. Kanai A, editor. PLoS ONE. Public Library of Science; 2012;7: e43031.
844 doi:10.1371/journal.pone.0043031

845 38. Abernathy E, Gilbertson S, Alla R, Glaunsinger B. Viral Nucleases Induce an mRNA
846 Degradation-Transcription Feedback Loop in Mammalian Cells. Cell Host and Microbe.
847 2015;18: 243–253. doi:10.1016/j.chom.2015.06.019

848 39. Núñez RD, Budt M, Saenger S, Paki K, Arnold U, Sadewasser A, et al. The RNA
849 Helicase DDX6 Associates with RIG-I to Augment Induction of Antiviral Signaling. Int
850 J Mol Sci. Multidisciplinary Digital Publishing Institute; 2018;19: 1877.
851 doi:10.3390/ijms19071877

852 40. Balinsky CA, Schmeisser H, Wells AI, Ganesan S, Jin T, Singh K, et al. IRAV
853 (FLJ11286), an Interferon-Stimulated Gene with Antiviral Activity against Dengue
854 Virus, Interacts with MOV10. Diamond MS, editor. J Virol. 2017;91: 504.
855 doi:10.1128/JVI.01606-16

856 41. Wang H, Chang L, Wang X, Su A, Feng C, Fu Y, et al. MOV10 interacts with
857 Enterovirus 71 genomic 5'UTR and modulates viral replication. Biochem Biophys Res
858 Commun. 2016;479: 571–577. doi:10.1016/j.bbrc.2016.09.112

859 42. Cuevas RA, Ghosh A, Wallerath C, Hornung V, Coyne CB, Sarkar SN. MOV10
860 Provides Antiviral Activity against RNA Viruses by Enhancing RIG-I-MAVS-
861 Independent IFN Induction. J Immunol. 2016;196: 3877–3886.
862 doi:10.4049/jimmunol.1501359

863 43. Burdick R, Smith JL, Chaipan C, Friew Y, Chen J, Venkatachari NJ, et al. P body-
864 associated protein Mov10 inhibits HIV-1 replication at multiple stages. J Virol. 2010;84:
865 10241–10253. doi:10.1128/JVI.00585-10

866 44. Burgess HM, Mohr I. Cellular 5“-3” mRNA exonuclease Xrn1 controls double-stranded
867 RNA accumulation and anti-viral responses. Cell Host and Microbe. 2015;17: 332–344.
868 doi:10.1016/j.chom.2015.02.003

869 45. Lumb JH, Li Q, Popov LM, Ding S, Keith MT, Merrill BD, et al. DDX6 Represses
870 Aberrant Activation of Interferon- Stimulated Genes. CellReports. ElsevierCompany;
871 2017;20: 819–831. doi:10.1016/j.celrep.2017.06.085

872 46. V'kovski P, Kratzel A, Steiner S, Stalder H, Thiel V. Coronavirus biology and
873 replication: implications for SARS-CoV-2. Nat Rev Microbiol. Nature Publishing
874 Group; 2020;5: 536–16. doi:10.1038/s41579-020-00468-6

875 47. Cui J, Li F, Shi Z-L. Origin and evolution of pathogenic coronaviruses. Springer US;
876 2019;: 1–12. doi:10.1038/s41579-018-0118-9

877 48. Banerjee A, Doxey AC, Tremblay BJ-M, Mansfield MJ, Subudhi S, Hirota JA, et al.
878 Predicting the recombination potential of severe acute respiratory syndrome coronavirus
879 2 and Middle East respiratory syndrome coronavirus. J Gen Virol. Microbiology
880 Society; 2020;101: 1251–1260. doi:10.1099/jgv.0.001491

881 49. Banerjee A, Doxey AC, Mossman K, Irving AT. Unraveling the Zoonotic Origin and
882 Transmission of SARS-CoV-2. Trends Ecol Evol. 2021;36: 180–184.
883 doi:10.1016/j.tree.2020.12.002

884 50. Zhou H, Ji J, Chen X, Bi Y, Li J, Wang Q, et al. Identification of novel bat
885 coronaviruses sheds light on the evolutionary origins of SARS-CoV-2 and related
886 viruses. Cell. 2021;184: 4380–4391.e14. doi:10.1016/j.cell.2021.06.008

887 51. Li W, Shi Z, Yu M, Ren W, Smith C, Epstein JH, et al. Bats are natural reservoirs of
888 SARS-like coronaviruses. Science. American Association for the Advancement of
889 Science; 2005;310: 676–679. doi:10.1126/science.1118391

890 52. Fielding CA, Jones GW, McLoughlin RM, McLeod L, Hammond VJ, Uceda J, et al.
891 Interleukin-6 signaling drives fibrosis in unresolved inflammation. Immunity. 2014;40:
892 40–50. doi:10.1016/j.immuni.2013.10.022

893 53. Blanco-Melo D, tenover BR. Imbalanced host response to SARS-CoV-2 drives
894 development of COVID-19. Cell. 2020;: 1–46. doi:10.1016/j.cell.2020.04.026

895 54. Pedersen SF, Ho Y-C. SARS-CoV-2: a storm is raging. Journal of Clinical Investigation.
896 2020;130: 2202–2205. doi:10.1172/JCI137647

897 55. Zou L, Ruan F, Huang M, Liang L, Huang H, Hong Z, et al. SARS-CoV-2 Viral Load in
898 Upper Respiratory Specimens of Infected Patients. N Engl J Med. Massachusetts
899 Medical Society; 2020;382: 1177–1179. doi:10.1056/NEJMc2001737

900 56. Libby P, Lüscher T. COVID-19 is, in the end, an endothelial disease. Eur Heart J. 3rd
901 ed. 2020;41: 3038–3044. doi:10.1093/eurheartj/ehaa623

902 57. Chen G, Wu D, Guo W, Cao Y, Huang D, Wang H, et al. Clinical and immunological
903 features of severe and moderate coronavirus disease 2019. J Clin Invest. American
904 Society for Clinical Investigation; 2020;130: 2620–2629. doi:10.1172/JCI137244

905 58. Pons S, Fodil S, Azoulay E, Zafrani L. The vascular endothelium: the cornerstone of
906 organ dysfunction in severe SARS-CoV-2 infection. Crit Care. BioMed Central;
907 2020;24: 353–8. doi:10.1186/s13054-020-03062-7

908 59. Lowenstein CJ, Solomon SD. Severe COVID-19 is a Microvascular Disease.
909 Circulation. Lippincott Williams & Wilkins Hagerstown, MD; 2020;191: 148.
910 doi:10.1161/CIRCULATIONAHA.120.050354

911 60. Varga Z, Flammer AJ, Steiger P, Haberecker M, Andermatt R, Zinkernagel AS, et al.
912 Endothelial cell infection and endotheliitis in COVID-19. The Lancet. Elsevier Ltd;
913 2020;395: 1417–1418. doi:10.1016/S0140-6736(20)30937-5

914 61. Amraei R, Rahimi N. COVID-19, Renin-Angiotensin System and Endothelial
915 Dysfunction. Cells. Multidisciplinary Digital Publishing Institute; 2020;9: 1652.
916 doi:10.3390/cells9071652

917 62. Teuwen L-A, Geldhof V, Pasut A, Carmeliet P. COVID-19: the vasculature unleashed.
918 Nature Reviews Immunology. Nature Publishing Group; 2020;20: 389–391.
919 doi:10.1038/s41577-020-0343-0

920 63. Gu SX, Tyagi T, Jain K, Gu VW, Lee SH, Hwa JM, et al. Thrombocytopathy and
921 endotheliopathy: crucial contributors to COVID-19 thromboinflammation. Nat Rev
922 Cardiol. Nature Publishing Group; 2021;18: 194–209. doi:10.1038/s41569-020-00469-1

923 64. Suvorava T, Kaesemeyer W. Targeting the Vascular Endothelium in the Treatment of
924 COVID-19. J Cardiovasc Pharmacol. 2021;77: 1–3.
925 doi:10.1097/FJC.0000000000000932

926 65. Bastard P, Rosen LB, Zhang Q, Michailidis E, Hoffmann H-H, Zhang Y, et al. Auto-
927 antibodies against type I IFNs in patients with life-threatening COVID-19. Science.
928 2020;129: eabd4585. doi:10.1126/science.abd4585

929 66. Zhang Q, Bastard P, Liu Z, Le Pen J, Moncada-Velez M, Chen J, et al. Inborn errors of
930 type I IFN immunity in patients with life-threatening COVID-19. Science. 2020;:
931 eabd4570. doi:10.1126/science.abd4570

932 67. Park A, Iwasaki A. Type I and Type III Interferons - Induction, Signaling, Evasion, and
933 Application to Combat COVID-19. Cell Host and Microbe. 2020;27: 870–878.
934 doi:10.1016/j.chom.2020.05.008

935 68. Thorne LG, Bouhaddou M, Reuschl A-K, Zuliani-Alvarez L, Polacco B, Pelin A, et al.
936 Evolution of enhanced innate immune evasion by the SARS-CoV-2 B.1.1.7 UK variant.
937 bioRxiv. Cold Spring Harbor Laboratory; 2021;: 2021.06.06.446826.
938 doi:10.1101/2021.06.06.446826

939 69. Sposito B, Broggi A, Pandolfi L, Crotta S, Clementi N, Ferrarese R, et al. The interferon
940 landscape along the respiratory tract impacts the severity of COVID-19. Cell. 2021;184:
941 4953–4968.e16. doi:10.1016/j.cell.2021.08.016

942 70. Ziegler CGK, Miao VN, Owings AH, Navia AW, Tang Y, Bromley JD, et al. Impaired
943 local intrinsic immunity to SARS-CoV-2 infection in severe COVID-19. Cell. 2021;184:
944 4713–4733.e22. doi:10.1016/j.cell.2021.07.023

945 71. Zhou Z, Ren L, Zhang L, Zhong J, Xiao Y, Jia Z, et al. Heightened Innate Immune
946 Responses in the Respiratory Tract of COVID-19 Patients. Cell Host and Microbe.
947 2020;27: 883–890.e2. doi:10.1016/j.chom.2020.04.017

948 72. Hadjadj J, Yatim N, Barnabei L, Corneau A, Boussier J, Smith N, et al. Impaired type I
949 interferon activity and inflammatory responses in severe COVID-19 patients. Science.
950 2020;369: 718–724. doi:10.1126/science.abc6027

951 73. Banerjee A, El-Sayes N, Budylowski P, Jacob RA, Richard D, Maan H, et al.
952 Experimental and natural evidence of SARS-CoV-2-infection-induced activation of type
953 I interferon responses. iScience. 2021;24: 102477. doi:10.1016/j.isci.2021.102477

954 74. Yuen C-K, Lam J-Y, Wong W-M, Mak L-F, Wang X, Chu H, et al. SARS-CoV-2
955 nsp13, nsp14, nsp15 and orf6 function as potent interferon antagonists. Emerging
956 Microbes & Infections. Taylor & Francis; 2020;9: 1418–1428.
957 doi:10.1080/22221751.2020.1780953

958 75. Miorin L, Kehrer T, Sanchez-Aparicio MT, Zhang K, Cohen P, Patel RS, et al. SARS-
959 CoV-2 Orf6 hijacks Nup98 to block STAT nuclear import and antagonize interferon
960 signaling. Proc Natl Acad Sci USA. 2020;5: 202016650–11.
961 doi:10.1073/pnas.2016650117

962 76. Banerjee AK, Blanco MR, Bruce EA, Honson DD, Chen LM, Chow A, et al. SARS-
963 CoV-2 disrupts splicing, translation, and protein trafficking to suppress host defenses.
964 Cell. Elsevier Inc; 2020;: 1–66. doi:10.1016/j.cell.2020.10.004

965 77. Konno Y, Kimura I, Uriu K, Fukushi M, Irie T, Koyanagi Y, et al. SARS-CoV-2 ORF3b
966 Is a Potent Interferon Antagonist Whose Activity Is Increased by a Naturally Occurring
967 Elongation Variant. CellReports. 2020;32: 108185. doi:10.1016/j.celrep.2020.108185

968 78. Yin X, Riva L, Pu Y, Martin-Sancho L, Kanamune J, Yamamoto Y, et al. MDA5
969 Governs the Innate Immune Response to SARS-CoV-2 in Lung Epithelial Cells.
970 CellReports. 2021;34: 108628. doi:10.1016/j.celrep.2020.108628

971 79. Lei X, Dong X, Ma R, Wang W, Xiao X, Tian Z, et al. Activation and evasion of type I
972 interferon responses by SARS-CoV-2. Nature Communications. Nature Publishing
973 Group; 2020;11: 3810–12. doi:10.1038/s41467-020-17665-9

974 80. Beyer DK, Forero A. Mechanisms of Antiviral Immune Evasion of SARS-CoV-2. J Mol
975 Biol. 2021;: 167265. doi:10.1016/j.jmb.2021.167265

976 81. Xia H, Cao Z, Xie X, Zhang X, Chen JY-C, Wang H, et al. Evasion of Type I Interferon
977 by SARS-CoV-2. CellReports. 2020;33: 108234. doi:10.1016/j.celrep.2020.108234

978 82. Suryawanshi RK, Koganti R, Agelidis A, Patil CD, Shukla D. Dysregulation of Cell
979 Signaling by SARS-CoV-2. Trends in Microbiology. 2021;29: 224–237.
980 doi:10.1016/j.tim.2020.12.007

981 83. Wickenhagen A, Sugrue E, Lytras S, Kuchi S, Noerenberg M, Turnbull ML, et al. A
982 prenylated dsRNA sensor protects against severe COVID-19. Science. American
983 Association for the Advancement of Science; 2021;: eabj3624.
984 doi:10.1126/science.abj3624

985 84. Hsu JC-C, Laurent-Rolle M, Pawlak JB, Wilen CB, Cresswell P. Translational shutdown
986 and evasion of the innate immune response by SARS-CoV-2 NSP14 protein. Proc Natl
987 Acad Sci USA. National Academy of Sciences; 2021;118.
988 doi:10.1073/pnas.2101161118

989 85. Zhao Y, Sui L, Wu P, Wang W, Wang Z, Yu Y, et al. A dual-role of SARS-CoV-2
990 nucleocapsid protein in regulating innate immune response. Signal Transduct Target
991 Ther. Nature Publishing Group; 2021;6: 331–14. doi:10.1038/s41392-021-00742-w

992 86. Sola I, Galán C, Mateos-Gómez PA, Palacio L, Zuñiga S, Cruz JL, et al. The
993 polypyrimidine tract-binding protein affects coronavirus RNA accumulation levels and
994 relocalizes viral RNAs to novel cytoplasmic domains different from replication-
995 transcription sites. J Virol. 3rd ed. 2011;85: 5136–5149. doi:10.1128/JVI.00195-11

996 87. Raaben M, Groot Koerkamp MJA, Rottier PJM, de Haan CAM. Mouse hepatitis
997 coronavirus replication induces host translational shutoff and mRNA decay, with
998 concomitant formation of stress granules and processing bodies. Cellular Microbiology.
999 2007;9: 2218–2229. doi:10.1111/j.1462-5822.2007.00951.x

1000 88. Ackermann M, Mentzer SJ, Kolb M, Jonigk D. Inflammation and Intussusceptive
1001 Angiogenesis in COVID-19: everything in and out of Flow. Eur Respir J. 2020;383:
1002 2003147. doi:10.1183/13993003.03147-2020

1003 89. Nascimento Conde J, Schutt WR, Gorbunova EE, Mackow ER. Recombinant ACE2
1004 Expression Is Required for SARS-CoV-2 To Infect Primary Human Endothelial Cells
1005 and Induce Inflammatory and Procoagulative Responses. Patton JT, editor. mBio.
1006 American Society for Microbiology; 2020;11. doi:10.1128/mBio.03185-20

1007 90. Castle EL, Robinson C-A, Douglas P, Rinker KD, Corcoran JA. Viral manipulation of a
1008 mechanoresponsive signaling axis disassembles processing bodies. Mol Cell Biol. 2021;:
1009 MCB0039921. doi:10.1128/MCB.00399-21

1010 91. Sola I, Almazán F, Zuñiga S, Enjuanes L. Continuous and Discontinuous RNA
1011 Synthesis in Coronaviruses. Annu Rev Virol. Annual Reviews; 2015;2: 265–288.
1012 doi:10.1146/annurev-virology-100114-055218

1013 92. Ayache J, Bénard M, Ernoult-Lange M, Minshall N, Standart N, Kress M, et al. P-body
1014 assembly requires DDX6 repression complexes rather than decay or Ataxin2/2L
1015 complexes. Matera AG, editor. Mol Biol Cell. The American Society for Cell Biology;
1016 2015;26: 2579–2595. doi:10.1091/mbc.E15-03-0136

1017 93. Gordon DE, Jang GM, Bouhaddou M, Xu J, Obernier K, White KM, et al. A SARS-
1018 CoV-2 protein interaction map reveals targets for drug repurposing. Nature. Nature
1019 Publishing Group; 2020;583: 459–468. doi:10.1038/s41586-020-2286-9

1020 94. Min Y-Q, Mo Q, Wang J, Deng F, Wang H, Ning Y-J. SARS-CoV-2 nsp1:
1021 Bioinformatics, Potential Structural and Functional Features, and Implications for
1022 Drug/Vaccine Designs. Front Microbiol. Frontiers; 2020;11: 587317.
1023 doi:10.3389/fmicb.2020.587317

1024 95. Zeng W, Liu G, Ma H, Zhao D, Yang Y, Liu M, et al. Biochemical characterization of
1025 SARS-CoV-2 nucleocapsid protein. Biochem Biophys Res Commun. 2020;527: 618–
1026 623. doi:10.1016/j.bbrc.2020.04.136

1027 96. Bai Z, Cao Y, Liu W, Li J. The SARS-CoV-2 Nucleocapsid Protein and Its Role in Viral
1028 Structure, Biological Functions, and a Potential Target for Drug or Vaccine Mitigation.
1029 Viruses. Multidisciplinary Digital Publishing Institute; 2021;13: 1115.
1030 doi:10.3390/v13061115

1031 97. Peng T-Y, Lee K-R, Tarn W-Y. Phosphorylation of the arginine/serine dipeptide-rich
1032 motif of the severe acute respiratory syndrome coronavirus nucleocapsid protein
1033 modulates its multimerization, translation inhibitory activity and cellular localization.
1034 FEBS J. John Wiley & Sons, Ltd; 2008;275: 4152–4163. doi:10.1111/j.1742-
1035 4658.2008.06564.x

1036 98. McBride R, van Zyl M, Fielding BC. The coronavirus nucleocapsid is a multifunctional
1037 protein. Viruses. Multidisciplinary Digital Publishing Institute; 2014;6: 2991–3018.
1038 doi:10.3390/v6082991

1039 99. Cong Y, Ulasli M, Schepers H, Mauthe M, V'kovski P, Kriegenburg F, et al.
1040 Nucleocapsid Protein Recruitment to Replication-Transcription Complexes Plays a
1041 Crucial Role in Coronaviral Life Cycle. Dutch RE, editor. J Virol. American Society for
1042 Microbiology Journals; 2020;94: 181. doi:10.1128/JVI.01925-19

1043 100. Lu S, Ye Q, Singh D, Villa E, Cleveland DW, Corbett KD. The SARS-CoV-2
1044 Nucleocapsid phosphoprotein forms mutually exclusive condensates with RNA and the
1045 membrane-associated M protein. bioRxiv. 2020;18: 479.
1046 doi:10.1101/2020.07.30.228023

1047 101. Cascarina SM, Ross ED. A proposed role for the SARS-CoV-2 nucleocapsid protein in
1048 the formation and regulation of biomolecular condensates. FASEB j. 2020;34: 9832–
1049 9842. doi:10.1096/fj.202001351

1050 102. Chen H, Cui Y, Han X, Hu W, Sun M, Zhang Y, et al. Liquid-liquid phase separation by
1051 SARS-CoV-2 nucleocapsid protein and RNA. Cell Res. Nature Publishing Group;
1052 2020;30: 1143–1145. doi:10.1038/s41422-020-00408-2

1053 103. Savastano A, Ibáñez de Opakua A, Rankovic M, Zweckstetter M. Nucleocapsid protein
1054 of SARS-CoV-2 phase separates into RNA-rich polymerase-containing condensates.

1055 Nature Communications. Nature Publishing Group; 2020;11: 6041–10.
1056 doi:10.1038/s41467-020-19843-1

1057 104. Iserman C, Roden CA, Boerneke MA, Sealfon RSG, McLaughlin GA, Jungreis I, et al.
1058 Genomic RNA Elements Drive Phase Separation of the SARS-CoV-2 Nucleocapsid.
1059 Mol Cell. 2020;80: 1078–1091.e6. doi:10.1016/j.molcel.2020.11.041

1060 105. Carlson CR, Asfaha JB, Ghent CM, Howard CJ, Hartooni N, Safari M, et al.
1061 Phosphoregulation of Phase Separation by the SARS-CoV-2 N Protein Suggests a
1062 Biophysical Basis for its Dual Functions. Mol Cell. 2020;80: 1092–1103.e4.
1063 doi:10.1016/j.molcel.2020.11.025

1064 106. Cubuk J, Alston JJ, Incicco JJ, Singh S, Stuchell-Brereton MD, Ward MD, et al. The
1065 SARS-CoV-2 nucleocapsid protein is dynamic, disordered, and phase separates with
1066 RNA. Nature Communications. Nature Publishing Group; 2021;12: 1936–17.
1067 doi:10.1038/s41467-021-21953-3

1068 107. Sa Ribero M, Jouvenet N, Dreux M, Nisole S. Interplay between SARS-CoV-2 and the
1069 type I interferon response. PLoS Pathogens. Public Library of Science; 2020;16:
1070 e1008737. doi:10.1371/journal.ppat.1008737

1071 108. Gori Savellini G, Anichini G, Gandolfo C, Cusi MG. SARS-CoV-2 N Protein Targets
1072 TRIM25-Mediated RIG-I Activation to Suppress Innate Immunity. Viruses.
1073 Multidisciplinary Digital Publishing Institute; 2021;13: 1439. doi:10.3390/v13081439

1074 109. Oliveira SC, de Magalhães MTQ, Homan EJ. Immunoinformatic Analysis of SARS-
1075 CoV-2 Nucleocapsid Protein and Identification of COVID-19 Vaccine Targets. Front
1076 Immunol. Frontiers; 2020;11: 587615. doi:10.3389/fimmu.2020.587615

1077 110. Parker MD, Lindsey BB, Leary S, Gaudieri S, Chopra A, Wyles M, et al. Subgenomic
1078 RNA identification in SARS-CoV-2 genomic sequencing data. Genome Res. Cold
1079 Spring Harbor Lab; 2021;31: 645–658. doi:10.1101/gr.268110.120

1080 111. Leary S, Gaudieri S, Parker MD, Chopra A, James I, Pakala S, et al. Generation of a
1081 Novel SARS-CoV-2 Sub-genomic RNA Due to the R203K/G204R Variant in
1082 Nucleocapsid: Homologous Recombination has Potential to Change SARS-CoV-2 at
1083 Both Protein and RNA Level. Pathog Immun. 2021;6: 27–49. doi:10.20411/pai.v6i2.460

1084 112. Saffran HA, Pare JM, Corcoran JA, Weller SK, Smiley JR. Herpes simplex virus
1085 eliminates host mitochondrial DNA. EMBO Rep. 2007;8: 188–193.
1086 doi:10.1038/sj.embor.7400878

1087 113. Corcoran JA, Saffran HA, Duguay BA, Smiley JR. Herpes simplex virus UL12.5 targets
1088 mitochondria through a mitochondrial localization sequence proximal to the N terminus.
1089 J Virol. 2009;83: 2601–2610. doi:10.1128/JVI.02087-08

1090 114. Gordon DE, Hiatt J, Bouhaddou M, Rezelj VV, Ulferts S, Braberg H, et al. Comparative
1091 host-coronavirus protein interaction networks reveal pan-viral disease mechanisms.
1092 Science. 2020;11: eabe9403–38. doi:10.1126/science.abe9403

1093 115. Nabeel-Shah S, Lee H, Ahmed N, Marcon E, Farhangmehr S, Pu S, et al. SARS-CoV-2
1094 Nucleocapsid protein attenuates stress granule formation and alters gene expression via
1095 direct interaction with host mRNAs. bioRxiv. Cold Spring Harbor Laboratory; 2020;:
1096 2020.10.23.342113. doi:10.1101/2020.10.23.342113

1097 116. Luo L, Li Z, Zhao T, Ju X, Ma P, Jin B, et al. SARS-CoV-2 nucleocapsid protein phase
1098 separates with G3BPs to disassemble stress granules and facilitate viral production. Sci
1099 Bull (Beijing). 2021;66: 1194–1204. doi:10.1016/j.scib.2021.01.013

1100 117. Zheng Z-Q, Wang S-Y, Xu Z-S, Fu Y-Z, Wang Y-Y. SARS-CoV-2 nucleocapsid
1101 protein impairs stress granule formation to promote viral replication. Cell Discov.
1102 Nature Publishing Group; 2021;7: 38–11. doi:10.1038/s41421-021-00275-0

1103 118. Wang J, Shi C, Xu Q, Yin H. SARS-CoV-2 nucleocapsid protein undergoes liquid-liquid
1104 phase separation into stress granules through its N-terminal intrinsically disordered
1105 region. Cell Discov. Nature Publishing Group; 2021;7: 5–5. doi:10.1038/s41421-020-
1106 00240-3

1107 119. Dougherty JD, Reineke LC, Lloyd RE. mRNA decapping enzyme 1a (Dcp1a)-induced
1108 translational arrest through protein kinase R (PKR) activation requires the N-terminal
1109 enabled vasodilator-stimulated protein homology 1 (EVH1) domain. J Biol Chem.
1110 2014;289: 3936–3949. doi:10.1074/jbc.M113.518191

1111 120. Schmidt N, Lareau CA, Keshishian H, Ganskih S, Schneider C, Hennig T, et al. The
1112 SARS-CoV-2 RNA-protein interactome in infected human cells. Nat Microbiol. Nature
1113 Publishing Group; 2021;6: 339–353. doi:10.1038/s41564-020-00846-z

1114 121. Tibble RW, Depaix A, Kowalska J, Jemielity J, Gross JD. Biomolecular condensates
1115 amplify mRNA decapping by coupling protein interactions with conformational changes
1116 in Dcp1/Dcp2. 2020;60th Anniversary: 600–36. doi:10.1101/2020.07.09.195057

1117 122. Tenekeci U, Poppe M, Beuerlein K, Buro C, Müller H, Weiser H, et al. K63-
1118 Ubiquitylation and TRAF6 Pathways Regulate Mammalian P-Body Formation and
1119 mRNA Decapping. Mol Cell. 2016;62: 943–957. doi:10.1016/j.molcel.2016.05.017

1120 123. Li Y, Chen R, Zhou Q, Xu Z, Li C, Wang S, et al. LSm14A is a processing body-
1121 associated sensor of viral nucleic acids that initiates cellular antiviral response in the
1122 early phase of viral infection. Proc Natl Acad Sci USA. 2012;109: 11770–11775.
1123 doi:10.1073/pnas.1203405109

1124 124. Rzeczkowski K, Beuerlein K, Müller H, Dittrich-Breiholz O, Schneider H, Kettner-
1125 Buhrow D, et al. c-Jun N-terminal kinase phosphorylates DCP1a to control formation of
1126 P bodies. J Cell Biol. 2011;194: 581–596. doi:10.1083/jcb.201006089

1127 125. Stoecklin G, Mayo T, Anderson P. ARE-mRNA degradation requires the 5“-3” decay
1128 pathway. EMBO Rep. 2006;7: 72–77. doi:10.1038/sj.embor.7400572

1129 126. Banerjee A, Nasir JA, Budylowski P, Yip L, Aftanas P, Christie N, et al. Isolation,
1130 Sequence, Infectivity, and Replication Kinetics of Severe Acute Respiratory Syndrome
1131 Coronavirus 2. Emerging Infect Dis. 2020;26: 2054–2063. doi:10.3201/eid2609.201495

1132 127. Mendoza EJ, Manguiat K, Wood H, Drebot M. Two Detailed Plaque Assay Protocols
1133 for the Quantification of Infectious SARS-CoV-2. Curr Protoc Microbiol. John Wiley &
1134 Sons, Ltd; 2020;57: cpmc105. doi:10.1002/cpmc.105

1135 128. Kamentsky L, Jones TR, Fraser A, Bray M-A, Logan DJ, Madden KL, et al. Improved
1136 structure, function and compatibility for CellProfiler: modular high-throughput image
1137 analysis software. Bioinformatics. 2011;27: 1179–1180.
1138 doi:10.1093/bioinformatics/btr095

1139 129. Johnston BP, Pringle ES, McCormick C. KSHV activates unfolded protein response
1140 sensors but suppresses downstream transcriptional responses to support lytic replication.
1141 Swaminathan S, editor. PLoS Pathogens. 2019;15: e1008185.
1142 doi:10.1371/journal.ppat.1008185

1143

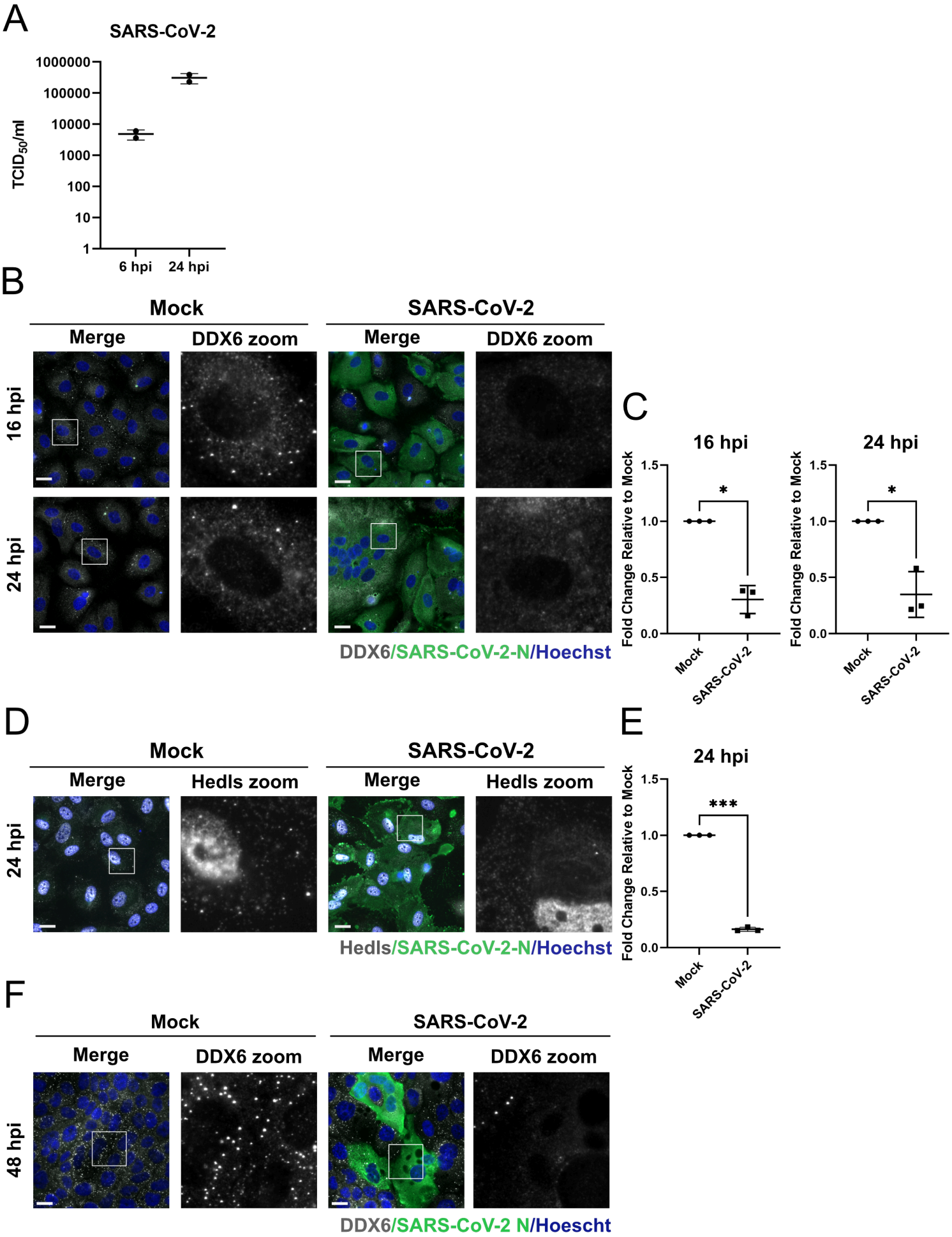
A
SARS-CoV-2
TCID50/ml
1000000
100000
10000
1000
100
10
1
6 hpi
24 hpi
B
Mock
SARS-CoV-2
Merge
DDX6 zoom
16 hpi
24 hpi
DDX6/SARS-CoV-2-N/Hoechst
C
16 hpi
24 hpi
Fold Change Relative to Mock
1.5
1.0
0.5
0.0
*
Mock
SARS-CoV-2
D
Hedls zoom
Hedls/SARS-CoV-2-N/Hoechst
E
***
F
48 hpi
DDX6/SARS-CoV-2 N/Hoescht

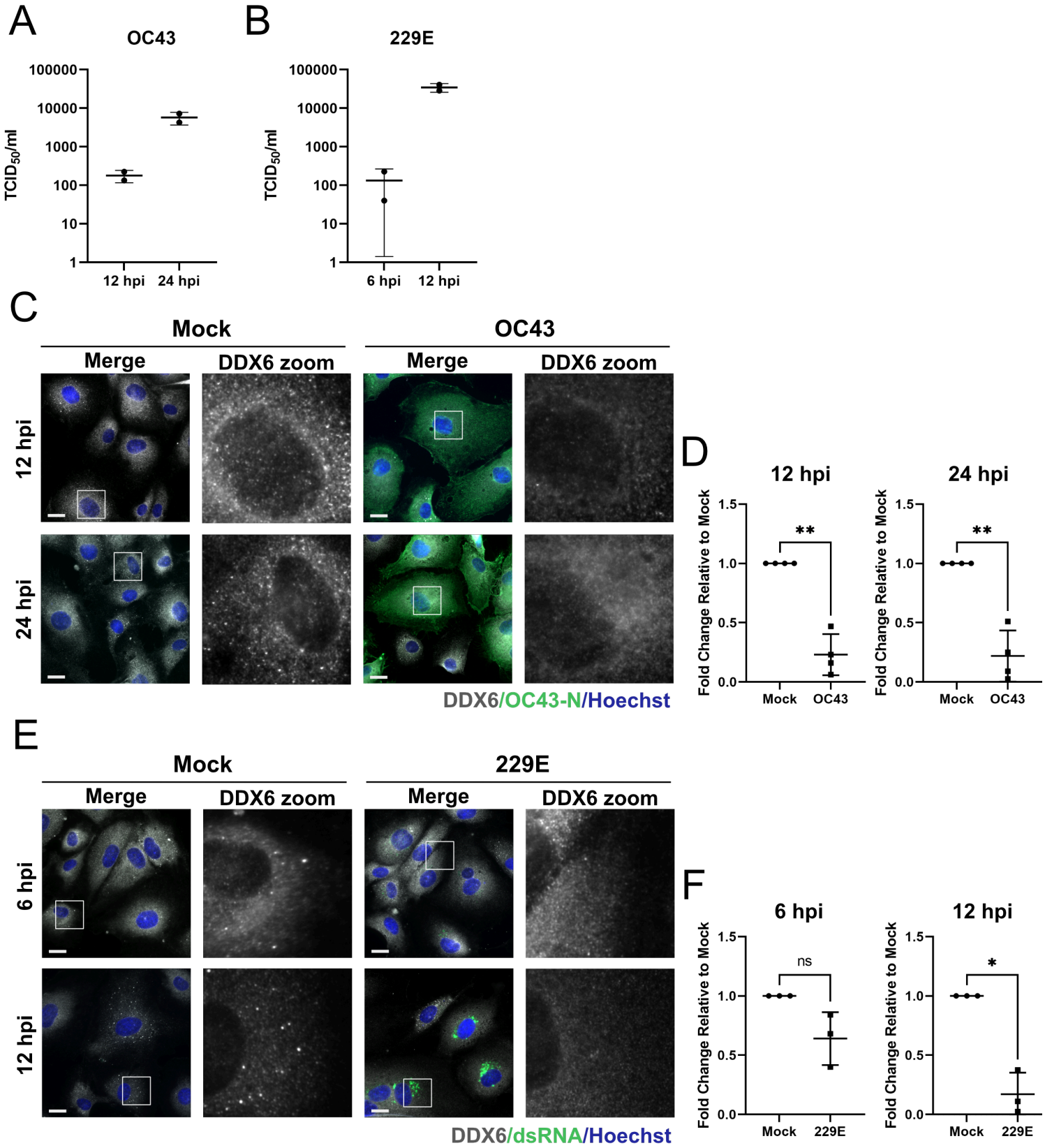
A
OC43
TCID50/ml
100000
10000
1000
100
10
1
12 hpi
24 hpi
B
229E
TCID50/ml
100000
10000
1000
100
10
1
6 hpi
12 hpi
C
Mock
OC43
Merge
DDX6 zoom
Merge
DDX6 zoom
12 hpi
24 hpi
DDX6/OC43-N/Hoechst
D
12 hpi
24 hpi
Fold Change Relative to Mock
1.5
1.0
0.5
0.0
**
Mock
OC43
E
Mock
229E
Merge
DDX6 zoom
Merge
DDX6 zoom
6 hpi
12 hpi
DDX6/dsRNA/Hoechst
F
6 hpi
12 hpi
Fold Change Relative to Mock
1.5
1.0
0.5
0.0
ns
*
Mock
229E

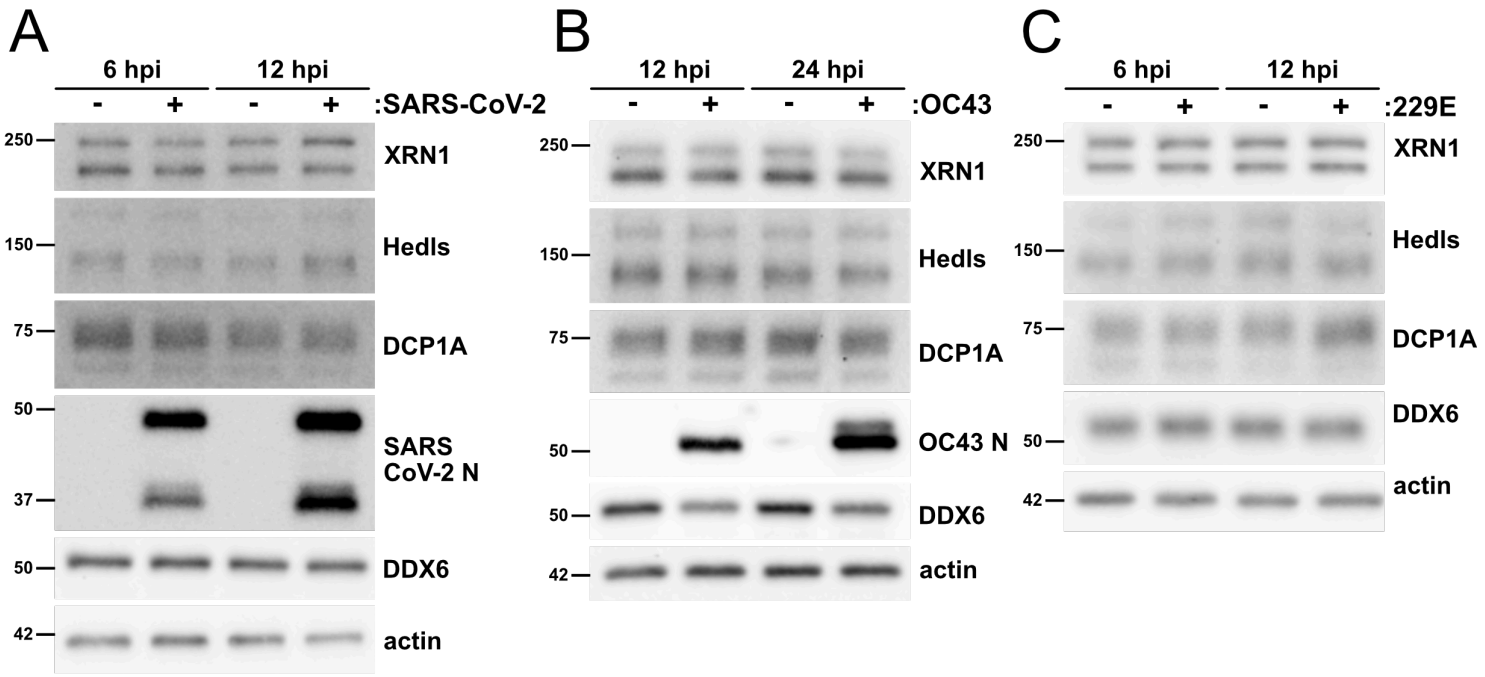
A
6 hpi
12 hpi
- + - + :SARS-CoV-2
250
150
75
50
37
50
42
XRN1
Hedls
DCP1A
SARS CoV-2 N
DDX6
actin
B
12 hpi
24 hpi
- + - + :OC43
250
150
75
50
50
42
XRN1
Hedls
DCP1A
OC43 N
DDX6
actin
C
6 hpi
12 hpi
- + - + :229E
250
150
75
50
42
XRN1
Hedls
DCP1A
DDX6
actin

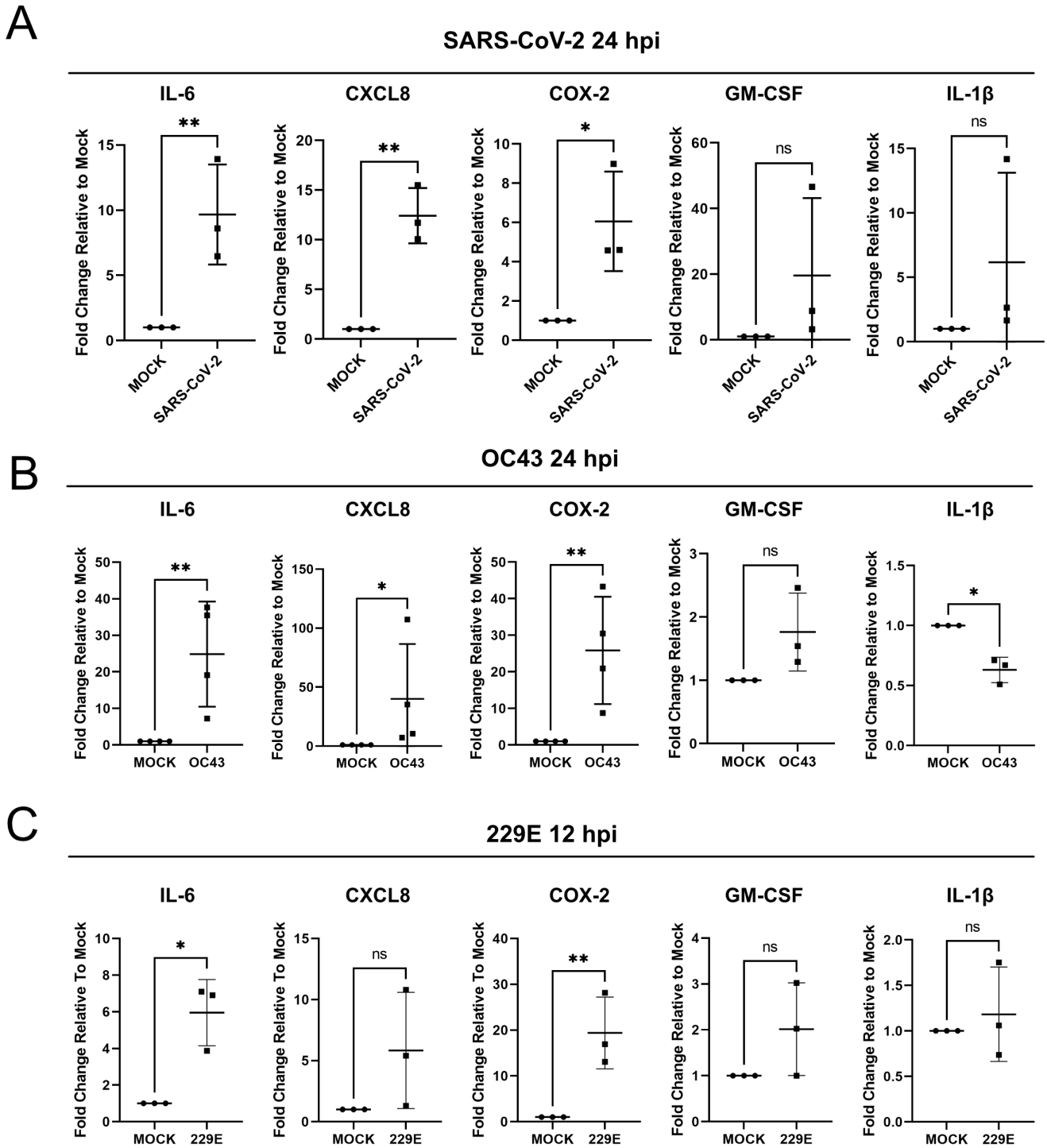
A
SARS-CoV-2 24 hpi
IL-6
CXCL8
COX-2
GM-CSF
IL-1β
Fold Change Relative to Mock
MOCK
SARS-CoV-2
**
*
ns
B
OC43 24 hpi
MOCK
OC43
C
229E 12 hpi
Fold Change Relative To Mock
229E

A

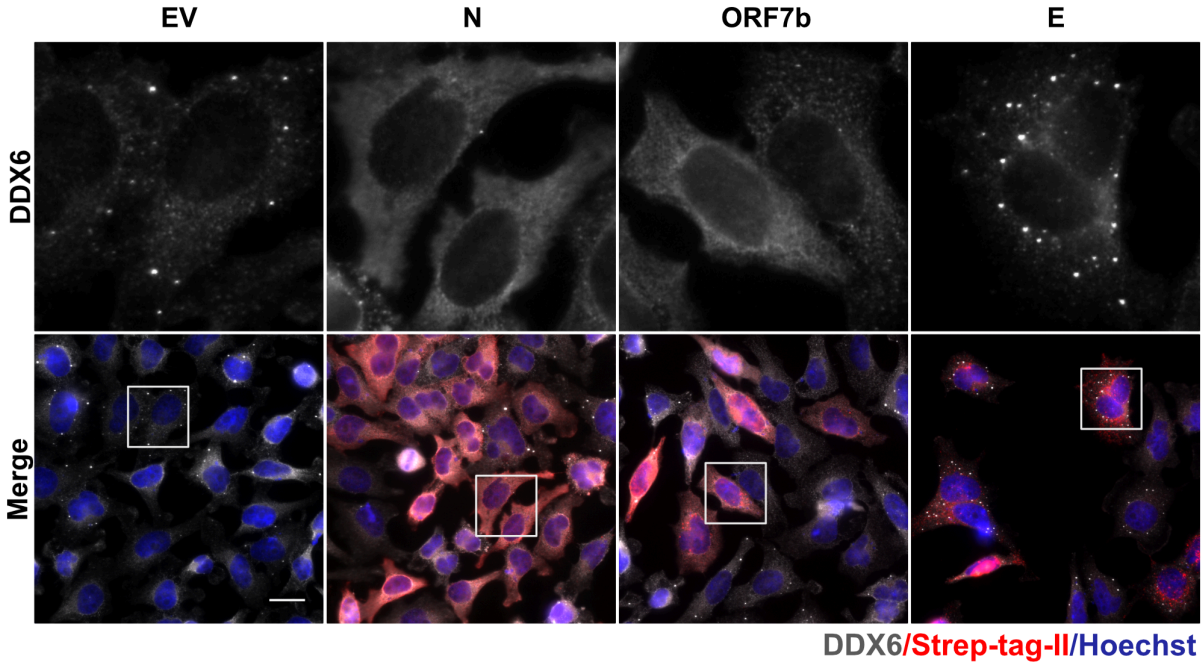
EV
N
ORF7b
E
DDX6
Merge
DDX6/Strep-tag-II/Hoechst

B

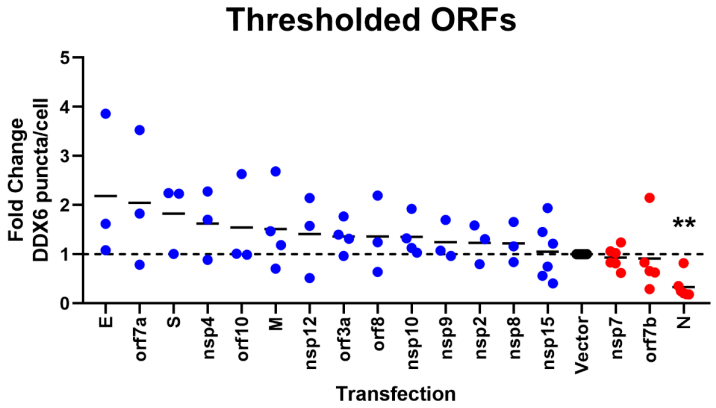
Thresholded ORFs
Fold Change DDX6 puncta/cell
0
1
2
3
4
5
**
E
orf7a
S
nsp4
orf10
M
nsp12
orf3a
orf8
nsp10
nsp9
nsp2
nsp8
nsp15
Vector
nsp7
orf7b
N
Transfection

C

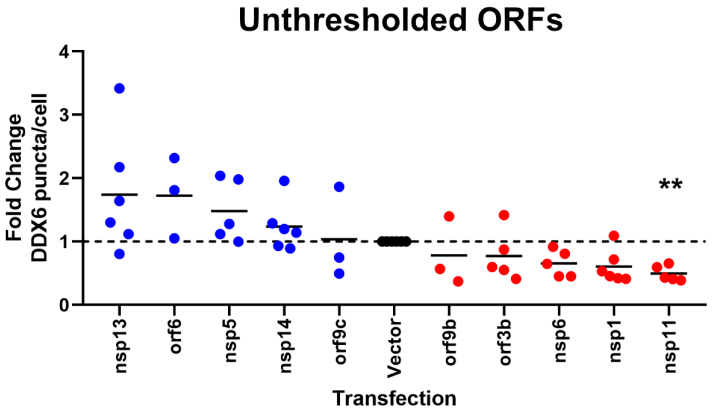
Unthresholded ORFs
Fold Change DDX6 puncta/cell
0
1
2
3
4
**
nsp13
orf6
nsp5
nsp14
orf9c
Vector
orf9b
orf3b
nsp6
nsp1
nsp11
Transfection

D

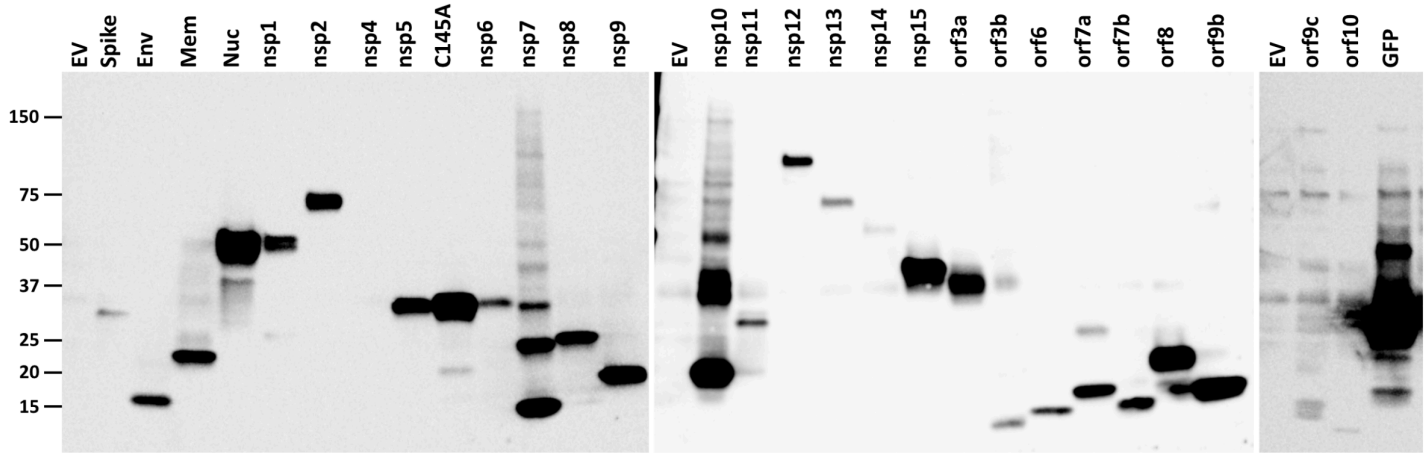
EV
Spike
Env
Mem
Nuc
nsp1
nsp2
nsp4
nsp5
C145A
nsp6
nsp7
nsp8
nsp9
EV
nsp10
nsp11
nsp12
nsp13
nsp14
nsp15
orf3a
orf3b
orf6
orf7a
orf7b
orf8
orf9b
EV
orf9c
orf10
GFP
150
75
50
37
25
20
15

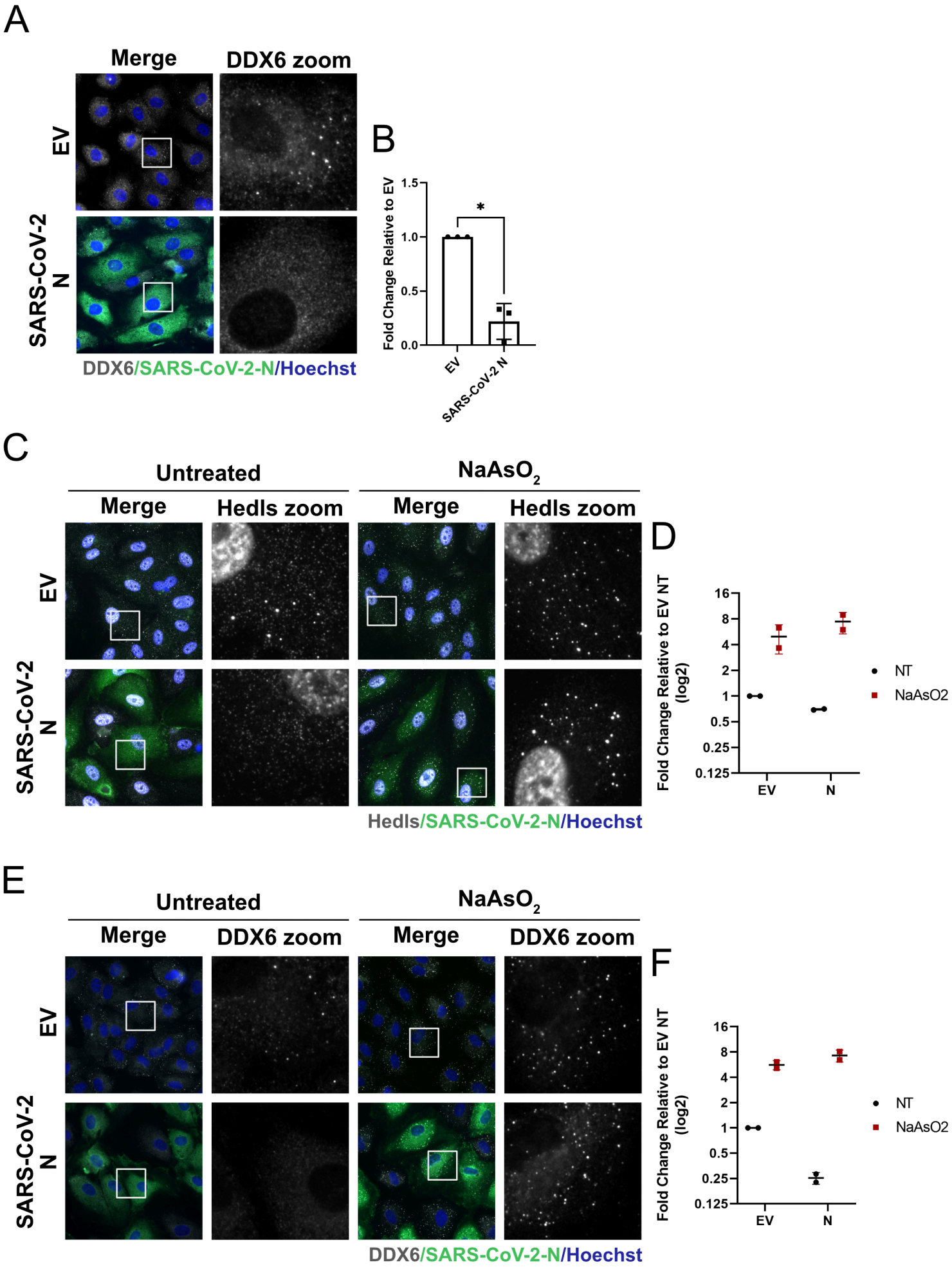
A
Merge
DDX6 zoom
EV
SARS-CoV-2 N
DDX6/SARS-CoV-2-N/Hoechst
B
Fold Change Relative to EV
1.5
1.0
0.5
0.0
*
EV
SARS-CoV-2 N
C
Untreated
NaAsO2
Merge
Hedls zoom
Merge
Hedls zoom
EV
SARS-CoV-2 N
Hedls/SARS-CoV-2-N/Hoechst
D
Fold Change Relative to EV NT (log2)
16
8
4
2
1
0.5
0.25
0.125
EV
N
NT
NaAsO2
E
Untreated
NaAsO2
Merge
DDX6 zoom
Merge
DDX6 zoom
EV
SARS-CoV-2 N
DDX6/SARS-CoV-2-N/Hoechst
F
Fold Change Relative to EV NT (log2)
16
8
4
2
1
0.5
0.25
0.125
EV
N
NT
NaAsO2

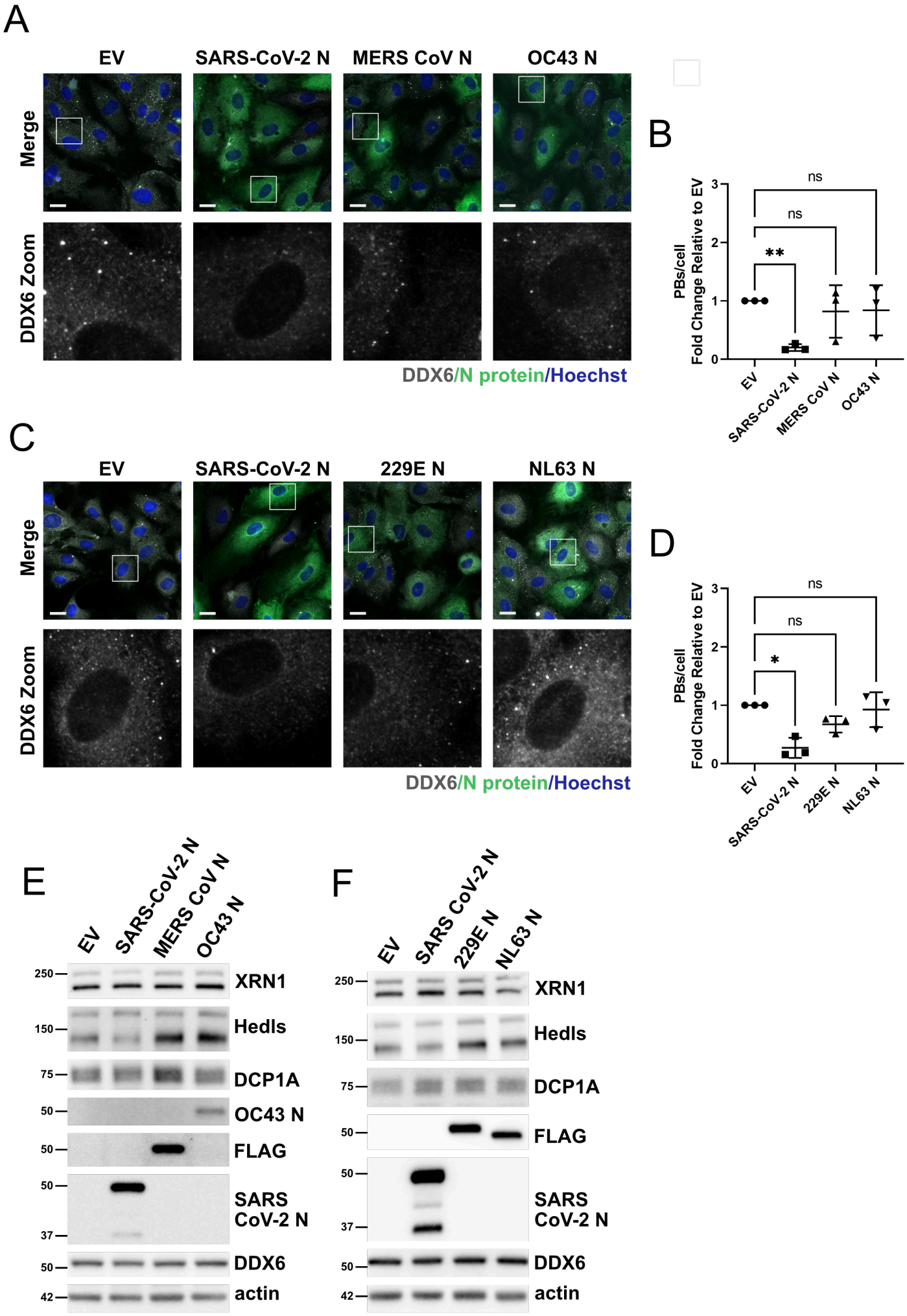
A
EV
SARS-CoV-2 N
MERS CoV N
OC43 N
Merge
DDX6 Zoom
DDX6/N protein/Hoechst
B
PBs/cell
Fold Change Relative to EV
ns
ns
**
EV
SARS-CoV-2 N
MERS CoV N
OC43 N
C
EV
SARS-CoV-2 N
229E N
NL63 N
Merge
DDX6 Zoom
DDX6/N protein/Hoechst
D
PBs/cell
Fold Change Relative to EV
ns
ns
*
EV
SARS-CoV-2 N
229E N
NL63 N
E
EV
SARS-CoV-2 N
MERS CoV N
OC43 N
250
XRN1
150
Hedls
75
DCP1A
50
OC43 N
50
FLAG
50
37
SARS CoV-2 N
50
DDX6
42
actin
F
EV
SARS CoV-2 N
229E N
NL63 N
250
XRN1
150
Hedls
75
DCP1A
50
FLAG
50
37
SARS CoV-2 N
50
DDX6
42
actin

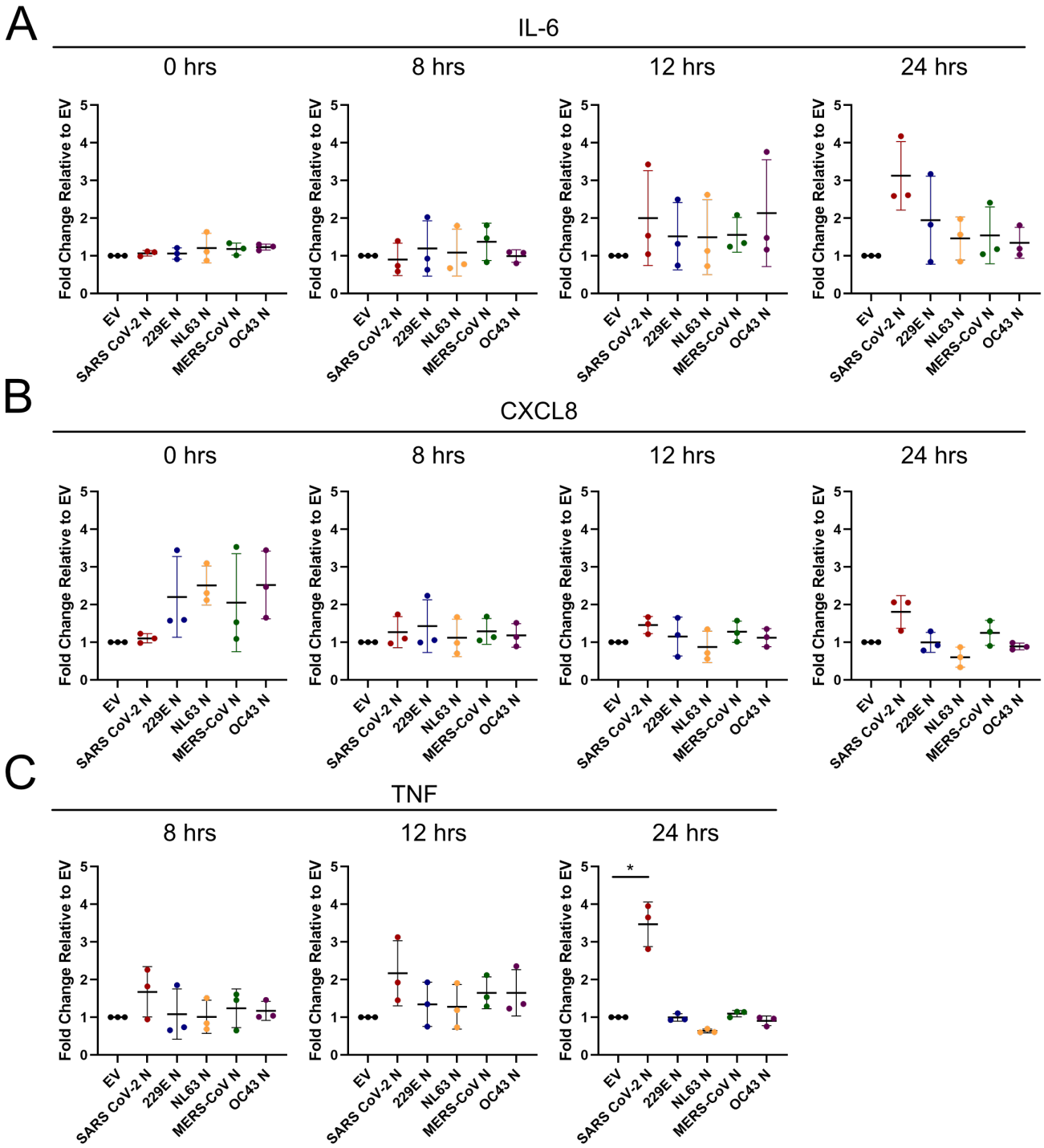
A
IL-6
0 hrs
8 hrs
12 hrs
24 hrs
B
CXCL8
0 hrs
8 hrs
12 hrs
24 hrs
C
TNF
8 hrs
12 hrs
24 hrs
Fold Change Relative to EV
0
1
2
3
4
5
*
EV
SARS CoV-2 N
229E N
NL63 N
MERS-CoV N
OC43 N

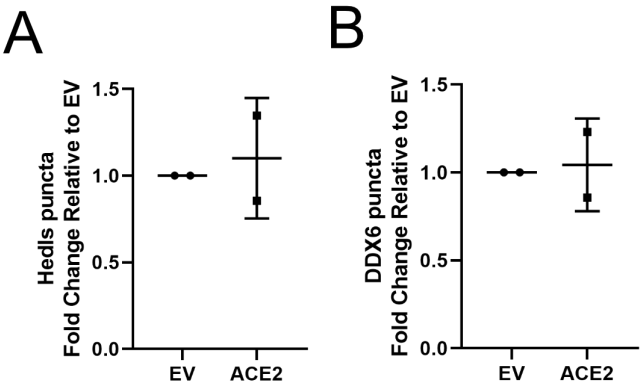
A
Hedls puncta
Fold Change Relative to EV
1.5
1.0
0.5
0.0
EV
ACE2
B
DDX6 puncta
Fold Change Relative to EV
1.5
1.0
0.5
0.0
EV
ACE2

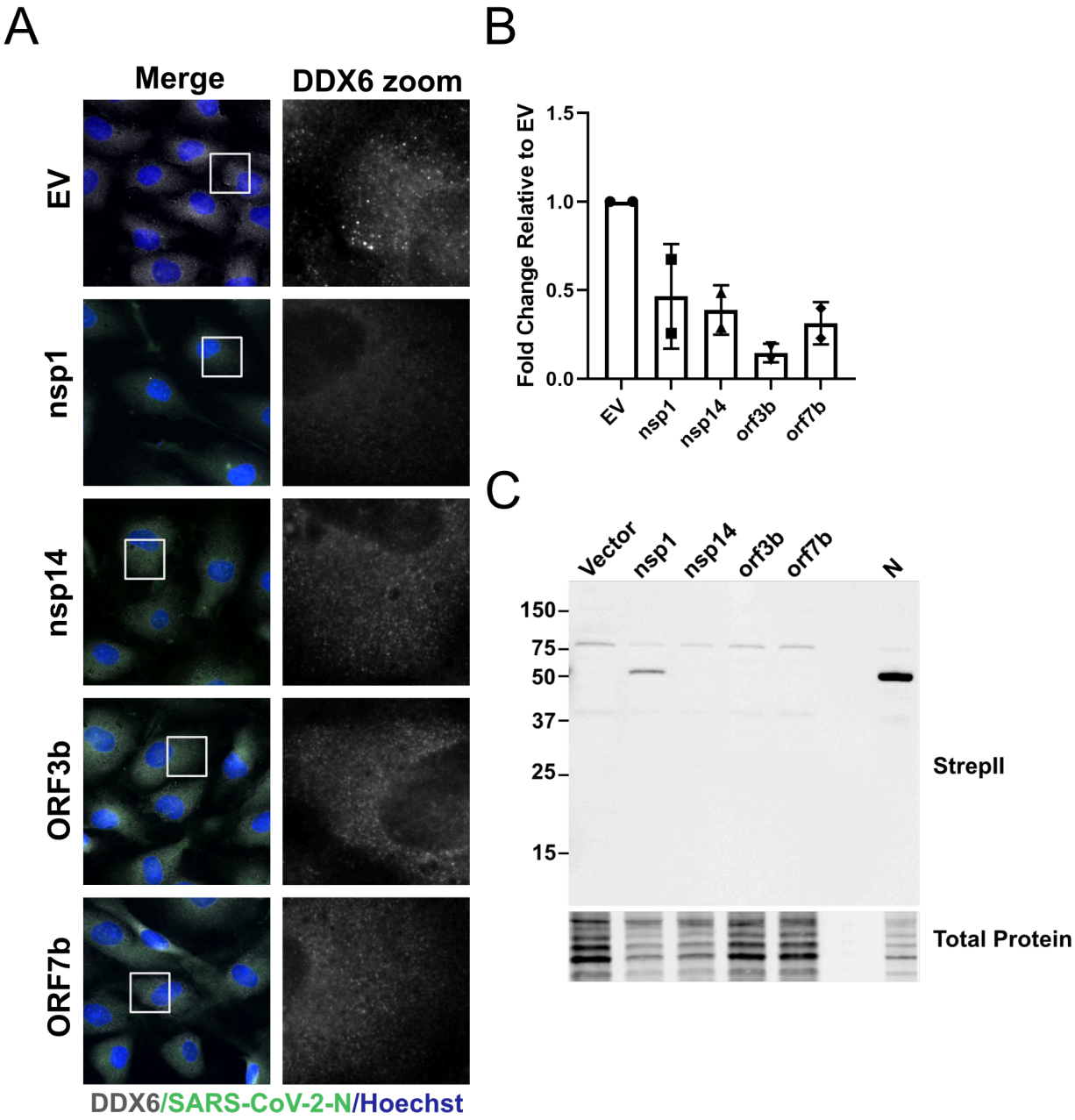
A
Merge
DDX6 zoom
EV
nsp1
nsp14
ORF3b
ORF7b
DDX6/SARS-CoV-2-N/Hoechst
B
Fold Change Relative to EV
1.5
1.0
0.5
0.0
EV
nsp1
nsp14
orf3b
orf7b
C
Vector
nsp1
nsp14
orf3b
orf7b
N
150
75
50
37
25
15
StrepII
Total Protein